TEMPERATURE DEPENDENCE OF LASER

INDUCED GRATINGS IN

EU-DOPED GLASSES

By

XIWANG ZHANG

Bachelor of Science

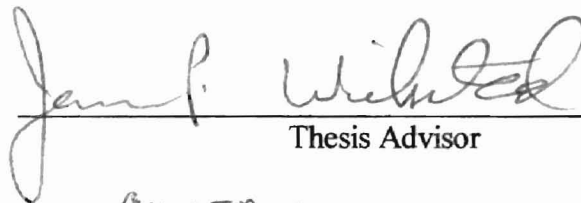University of Science and Technology of China

Hefei, Anhui

1996

Submitted to the Faculty of the
Graduate College of the
Oklahoma State University
in partial fulfillment of
the requirements for
the Degree of
MASTER OF SCIENCE
August, 2001

TEMPERATURE DEPENDENCE OF LASER

INDUCED GRATINGS IN

EU-DOPED GLASSES

Thesis Approved:

_____
Thesis Advisor

_____

_____

_____
Dean of the Graduate College

ACKNOWLEDGEMENTS

Chapter

BIBLIOG

APPE

Page

.... 60

J.J AI 62

TABLE OF CONTENTS

LIST OF TABLES

LIST OF FIGURES

I. Introduction:

In recent years, there has been a great deal of interest in laser induced gratings (LIG) written in rare-earth (RE) doped silicate glasses. This kind of laser induced grating is important because of its potential applications for optical devices, including holographic storage and holographic narrow-band rejection filters. [1, 2] In addition, since silicate glasses can be used to manufacture fibers, laser induced gratings can be integrated into fiber optic systems for applications in optical communication and sensors. [3]

These gratings are established by on-resonance or off-resonance excitation of the Eu^{3+} ions from the ground state $^7F_0$ to the excited state $^5D_2$ by using a four-wave-mixing (FWM) technique. [4, 5, 6, 7] They consist of two components. The transient component has been proved to be the population grating of excited Eu^{3+} rare-earth modifiers [8] since its decay rate is the same as that of the long-lived $^5D_0$ excited state. The mechanism to form the persistent gratings is still unclear, but it seems that hot phonons are driving the production of these persistent gratings. These hot phonons are produced by nonradiative relaxation of the rare-earth excited state. Several models have been provided to understand the formation of the persistent gratings. According to Powell *et al.* [8, 9, 10], a tunneling model is used to account for the formation of these gratings. The model is based on thermally induced changes in the local structure at the site of the Eu^{3+} ions. The basic assumption is that the network formers and modifier ions can arrange themselves

1

into two possible configurations that lead to different local environments around the Eu^{3+} ions. Each arrangement has a different refractive index, which results when the Eu^{3+} ions move from one potential well minimum to the other in a double-minima potential well. In 1997, Hamad et al. [11] presented a Bragg diffraction model for volume grating produced by two Gaussian beams in an absorbing medium. According to Dixon et al. [12], the persistent grating is attributed to the movement of small modifiers such as Na^+ and Mg^{2+} ions. The refractive-index contrast of the grating comes from the modulation of the concentration of small modifiers. The model includes diffusion driven by hot phonons from nonradiative relaxation of the rare-earth ions, drift under the space-charge field and trapping of the mobile modifiers.

Considerable research has been focused on the formation of persistent and transient grating in Eu^{3+} doped glasses at room temperature. However, until now, only a few studies on the temperature dependence of LIG formation in Eu^{3+} doped glasses have been reported. According to Behrens et al. [13], the results in the range of 160K and 370K in Eu^{3+} doped phosphate glasses showed a trend toward a higher laser-induced grating signal intensity as the temperature was lowered. French et al. [14] reported the temperature dependence of LIG in the Eu^{3+} doped silicate glasses at temperatures from 160K to 370K. This same trend was also found in their silicate glasses. But the time at which the grating signal intensity was measured is not clear. In the FWM experiments reported, it was found that the grating evolved as a function of time. So the time at which the scattering signal intensity was measured is important. Paxton [15] reported the results for the glass samples with the Eu_2O_3 concentration of 1.3% and 2.6% at three temperatures: 298K, 265K, and 238K. The following is the composition of the samples:

$[0.70SiO_2+0.15Na_2O+0.12MgO+0.03Al_2O_3](100-x)+xEu_2O_3$, where x=1.3 and 2.6. According to what he stated, there is a continuous monotonic increase for both samples at low temperatures. Later, Hamad [16] found that the monotonic increase of the signal was not due to volume LIG but due to a diffraction grating on a film deposited on the surface. This film was verified by studying the surface of the glass using an optical microscope. This effect was only observed at low temperature. The source of the film is still not clear.

The purpose of this thesis is to present the results of FWM experiments for glasses with various Eu_2O_3 content conducted below room temperature and above room temperature. The composition of the samples is $[0.70SiO_2+0.15Na_2O+0.12MgO+0.03Al_2O_3](100-x)+xEu_2O_3$, where x=2.6, 3.9, 5.3 and 8.1. The temperature of the experiments varied from -33°C to 93°C. In addition, several experiments were also conducted at liquid nitrogen temperature -196 °C. An entire procedure of a typical experimental curve can be divided into writing, blocking, erasing and rewriting processes. Experiments were performed to see how the temperature change influenced the characteristic parameters of grating intensity for each stage, such as the build up rate, initial maximum, decay rate and erasure rate of the laser induced grating.

CHAPTER 2

EXPERIMENT SETUP AND PROCEDURE

2.1 Experimental setup:

The experimental setup is presented in Fig. 1. The typical non-degenerate FWM technique was used to measure the intensity of the diffracted signal resulting from the laser induced gratings in several Eu^{3+}-doped dual alkaline silicate glasses. The two CW argon laser write beams that are split from the main laser beam intersect inside the sample with a crossing angle $2\theta_w$, which changes from $3.87°$, $5.145°$ to $8.75°$ (measured in air). The CW argon laser operating in the TEM_{00} mode radiated the 465.8 nm line, which excited the Eu^{3+} ions to the $^5D_2$ level. The power of the main laser beam is defined as P_w, which is about 50mW. By using the CCD camera, the diameter of each beam was measured to be 148μm at $2\theta_w=8.75°$, 156μm at $2\theta_w=3.87°$ and 144μm at $2\theta_w=5.145°$. To detect the grating, a He-Ne laser operating at 632.8 nm was used. The diameter of the read beam at the position of the sample is 180μm. The power of the read beam is defined as P_r, which is about 3mW. A photo-multiplier tube (PMT) was used to detect the diffracted signal. A calibration was conducted, which related the diffracted He-Ne laser power detected by the PMT to the number of counts per second. Therefore, by measuring the number of counts per second, we can obtain the intensity of the diffracted signal.

The temperature at which measurements were performed ranged from 93°C to liquid nitrogen temperature -196°C. The temperature was kept constant to within 1°C. Three dewars were used to conduct these temperature studies. To lower the temperature of the sample from room temperature, the sample was placed in a special dewar that was

4

He-Ne

M λ_w=465.8nm
w_w=74μm
P_w=50mW
λ_r=632.8nm
P_r=3mW
w_r=90μm

L

B

Sample

$2\theta_w$

L

L

N

I

PMT

M

Argon Laser

Figure 1. Experimental setup from Hamad *et al.* [7], $2\theta_w$=5.145°

a cube-shaped thermoelectric cryostat with a circular window on each side. To minimize the loss of the write, read and diffracted beams, the entrance and exit windows were coated with an anti-reflection coating. A Melcor multistage thermoelectric cooler was attached to the lid of the thermoelectric cryostat. A heat sink and fan were attached to the outer part of the lid to remove the heat from the thermoelectric cooler. The second dewar was used to raise the temperature of the sample to 93 °C. That dewar had the same shape as the previous one except that the entrance and exit windows had no anti-reflection coating. It was equipped with a heat element instead of a thermoelectric cooler. The third dewar was used to keep the sample at liquid nitrogen temperature. Instead of a thermoelectric cooler, it had a container, which was filled with liquid nitrogen. The heat conductivity between the plates holding the sample and the container was very high so that heat could be transferred between them effectively. After this container was filled with liquid nitrogen, the temperature of the sample was lowered and kept at the liquid nitrogen temperature. Before conducting an experiment, the dewar was pumped to approximately 2×10^{-6} Torr to eliminate condensation on the sample and windows. A Hewlett Packard 6633a DC power supply was used to supply the power for the thermoelectric cooler or heater. The temperature of the sample was probed by an Omega thermocouple, and a Hewlett Packard 3478A multimeter was used to monitor it. Several glass samples were made with different Eu^{3+} concentrations. The following is the composition of the samples: $[0.70SiO_2+0.15Na_2O+0.12MgO+0.03Al_2O_3](100-x)+xEu_2O_3$, where $x=2.6$, 3.9, 5.3, 8.1. Table 1 shows the identities and parameters of the samples required to calculate Δn. L is the thickness of the sample. α_w and α_r are the

Sample ID	Eu$_2$O$_3$ mol%	L (mm)	α_w (cm-1)	α_r (cm-1)	n_w	n_r	R (%)	β ($\times 10^5$)
Eu2.6	2.6	2.2	1.419	0.169	1.542	1.52	4.26	2.175
Eu3.9	3.9	3.26	2.036	0.266	1.545	1.52	4.26	1.656
Eu5.3	5.3	4.44	2.655	0.244	1.547	1.53	4.39	0.968
Eu8.1	8.1	2.02	4.471	0.289	1.58	1.56	4.79	1.191

Table 1. The parameters of the samples.

absorption coefficients at the wavelength of the write beam and read beam respectively. n_w and n_r are the index of refraction of the samples at the wavelength of the write beam and read beam respectively. R is reflectivity of the sample surface. β is the calculated value of $(\eta/\Delta n^2)$ from the Bragg diffraction model for volume grating proposed by Hamad *et al.* [11]. Appendix A describes this model in details.

2.2 Experimental procedure:

The experiments were performed according to the following procedures. The temperature of the sample was either lowered or raised by adjusting the voltage applied to the thermoelectric cooler or adding liquid nitrogen or adjusting the voltage applied to the heater. When the desired temperature was reached, both write beams were turned on to write the grating. The temperature was kept constant to within $1°C$ during the grating formation process. During each scan, a background signal was collected for the first 30-seconds. Then, the two write beams were turned on until the diffracted signal reached a maximum. After that, both write beams were blocked for five minutes. Then, one write beam was turned on to erase the grating. After the grating was almost entirely erased, another write beam was turned on, forming the grating again. This process lasted for about eight minutes. Finally, the write beams were blocked. A typical scan at room temperature is shown in Fig. 2, illustrating a typical evolution of the grating. Fig. 3 shows typical scans at three temperatures, $27.7°C$, $87°C$, and $-196°C$ for the sample Eu3.9.

To compare LIG strength among samples with different thickness and absorption coefficients, the change in the index of refraction Δn is calculated according to the model presented by Hamad *et al.* [11]. Appendix describes it in details. As Fig.2 shows, Δn

8
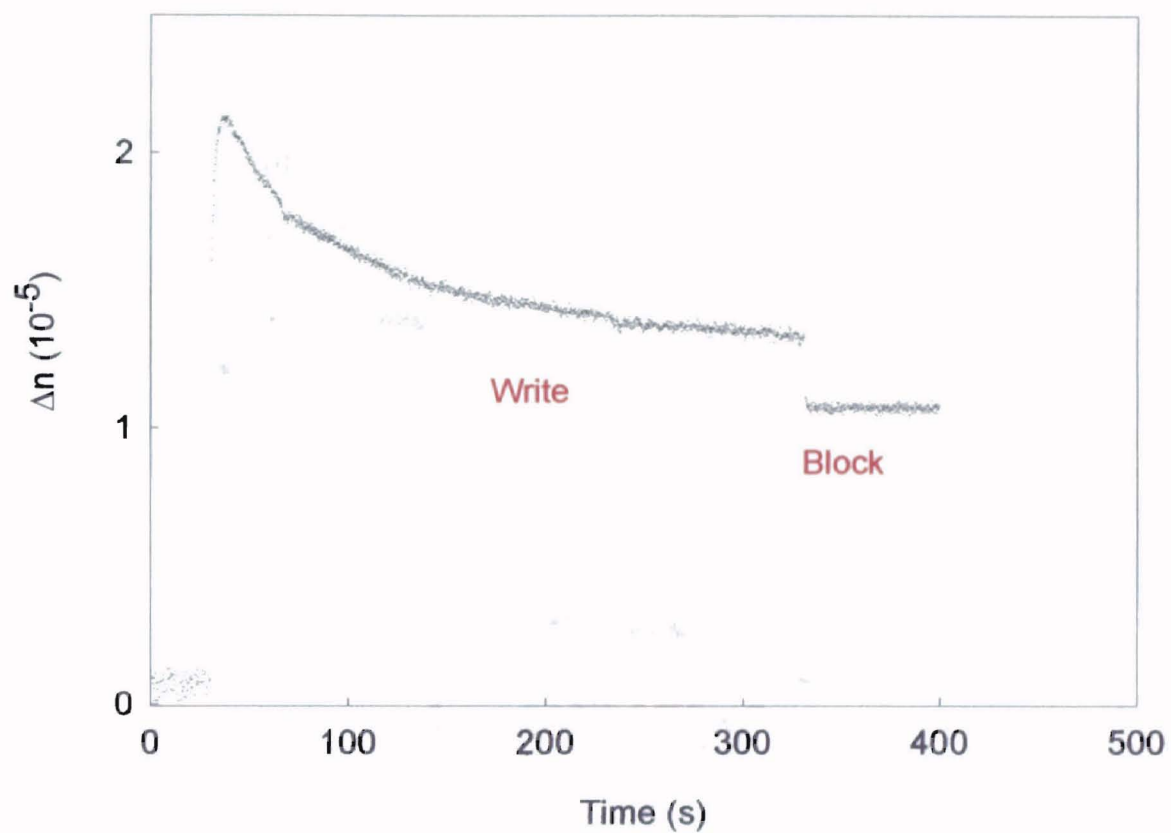
Figure 2. A typical scan of the sample Eu8.1, $P_w=50mW$, $P_r=2.7mW$, $2\theta_w=5.145°$, T=25.3 °C
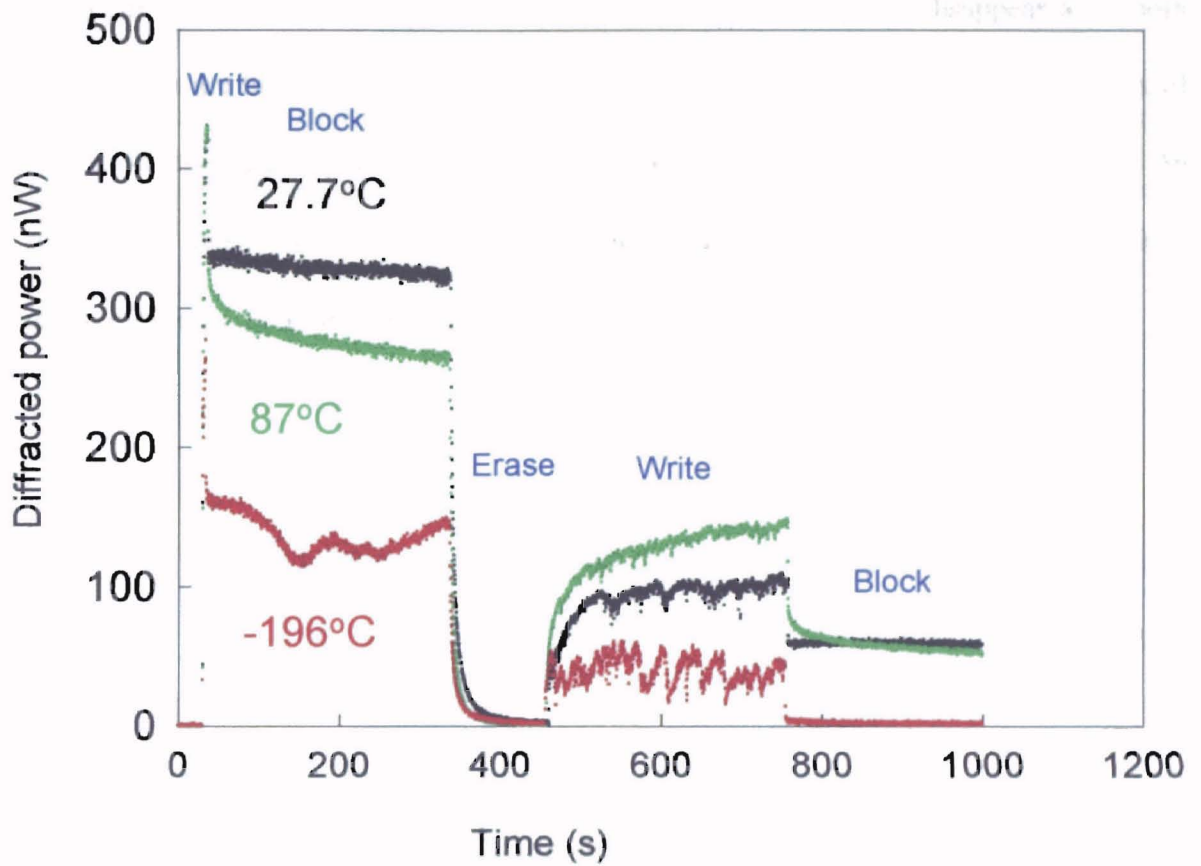
Figure 3. A typical scan for the sample Eu3.9, P_w=50mW, P_r=2.75mW, $2\theta_w$=8.75°

reaches the maximum and then decays. Fig. 3 shows that both write beams are blocked at the maximum. So Δn_{max} is defined as the maximum change in the index of refraction when Δn reaches the maximum. Because the transient grating will disappear after both write beams are blocked at the maximum, the maximum persistent change in the index of refraction $\Delta n_{persistent}$ is defined as the left change in the index of refraction just after Δn reaches the maximum. The transient change in the index of refraction $\Delta n_{transient}$ is defined as the difference between Δn_{max} and $\Delta n_{persistent}$.

CHAPTER 3

EXPERIMENT RESULTS

3.1 Power dependence of grating growth rate:

It can be expected that the laser induced grating grows faster with the larger power of the write beam, but the relation between the signal build-up rate and the power of the write beam is not obvious. Dixon *et al.* [12] presented a linear dependence result between the signal build-up rate and the power of the write beam at room temperature, but it is still not known whether this linear power dependence happens at other temperatures or not. To study the effect of the power of the write beam on the growth rate of the laser induced grating, the experiments were conducted on the Eu3.9 sample at $-33.2°C$ and on the Eu8.1 at $-196°C$, respectively. The power of the write beam varied in the range of 10 to 60 mW. The results are presented in Figs. 4. and 5. According to Dixon *et al.* [12], the signal build-up rate is measured by the reciprocal of the time that it takes to reach one-half the initial maximum of the diffracted signal intensity. These data show linear dependences for grating formation at low temperatures. The errors bar in Figs. 4 and 5 are the maximum ones of all points in Figs. 4 and 5 respectively.

3.2 Effects of Eu^{3+} concentration and temperature on the build-up time:

As Fig. 2 shows, the diffracted signal reaches the initial maximum, and then it begins to decay. The build-up time is defined as the time it takes for the signal to reach this initial maximum. How the build-up time changes with the Eu concentration and the
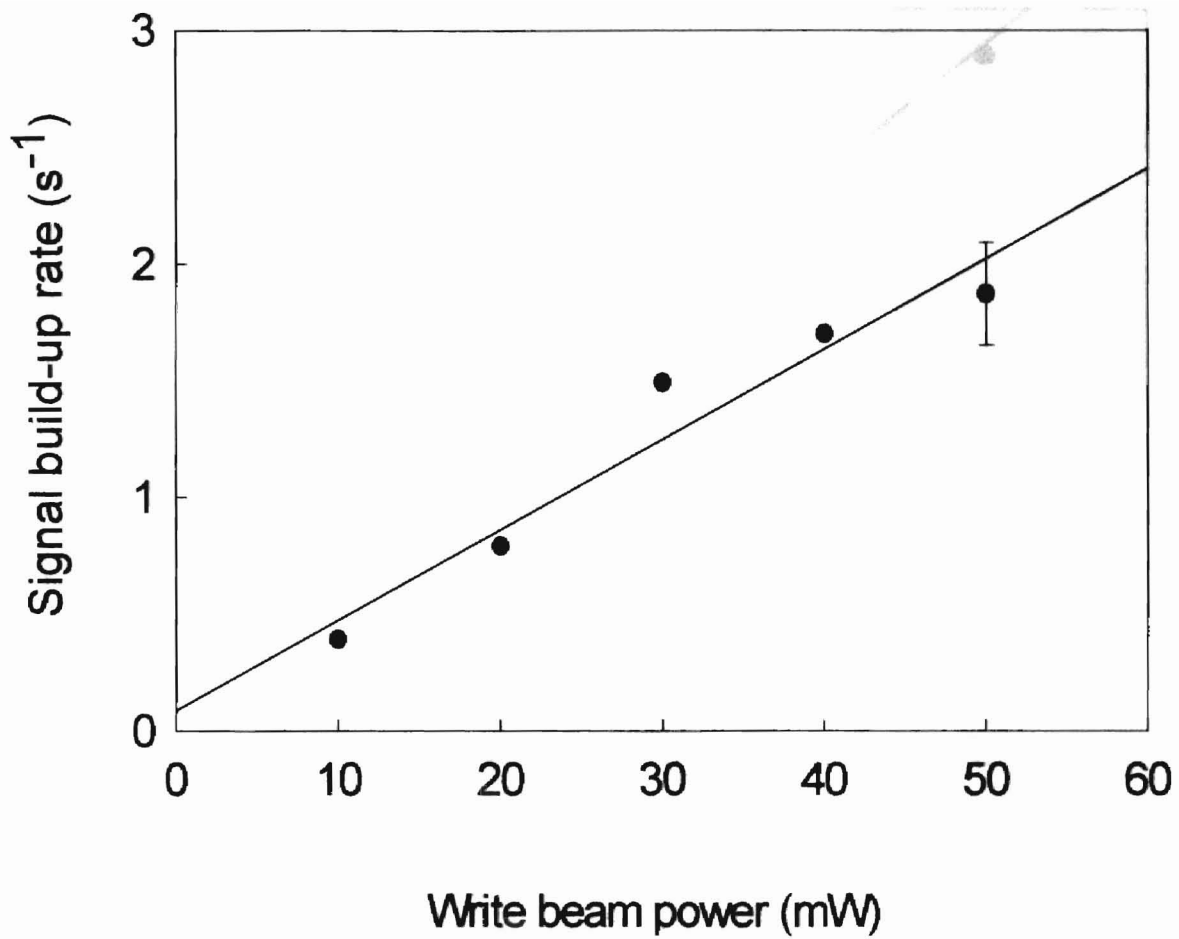
Figure 4. Power dependence of the growth rate of the gratings, Eu3.9,

T=-33.2 °C, $2\theta_w$=8.75 °
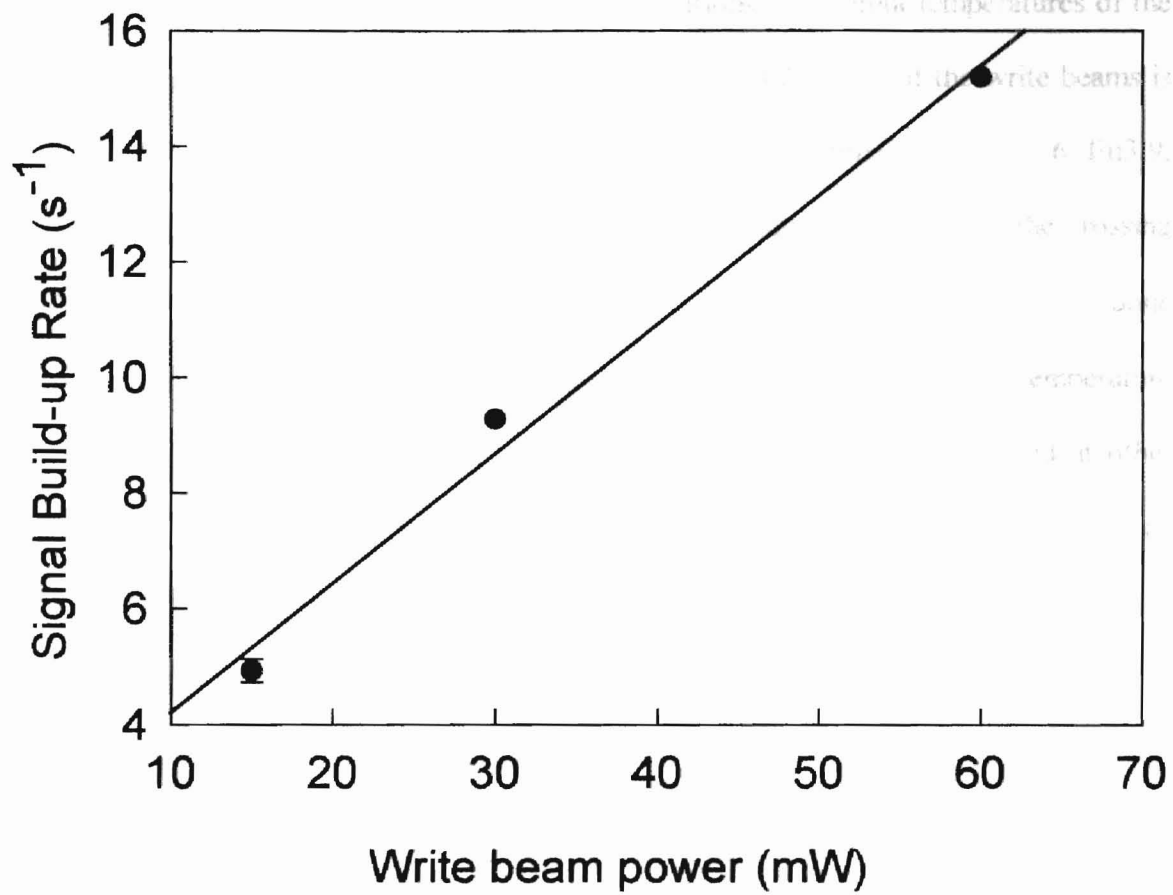
Figure 5. Power dependence of the growth rate of the gratings, Eu8.1,

T=-196 °C, $2\theta_w$=3.87 °

temperature is still not clear. To study the dependence of build-up time, experiments were conducted on samples with various Eu_2O_3 concentrations at different temperatures of the grating formation and at different crossing angles. The total power of the write beams is 50 mW in all cases. Fig. 6 presents the results of the build-up time for the Eu2.6, Eu3.9, Eu5.3 and Eu8.1 samples at different temperatures of grating formation at the crossing angle $2\theta_\omega = 5.145°$. This figure showed a broad temperature range since this is done systematically. As indicated by the figures, when the grating formation temperature increases, the build-up time increases. These experiments were also performed at other crossing angles such as $2\theta_\omega = 8.75°$. Fig. 7 presents the results of these measurements. Although these experiments have a narrower temperature range than those in Fig. 6, a similar trend is obtained. The error bars in Figs. 6 and 7 are the maximum ones of all measurements for each sample respectively.

3.3 Pre-exposure effects:

It was found that the initial diffraction maximum was lowered if one write beam was turned on for a certain period of time before the second write beam was turned on to form the grating. To study the effect of this pre-exposure, the experiments were performed on the Eu8.1 sample at room temperature with the crossing angle $2\theta_w = 5.145°$. The total write beam power was 50mW. Fig. 8 shows the results for pre-exposure times of 1s, 3 s and 8 s.

3.4 Temperature dependence of decay rate:
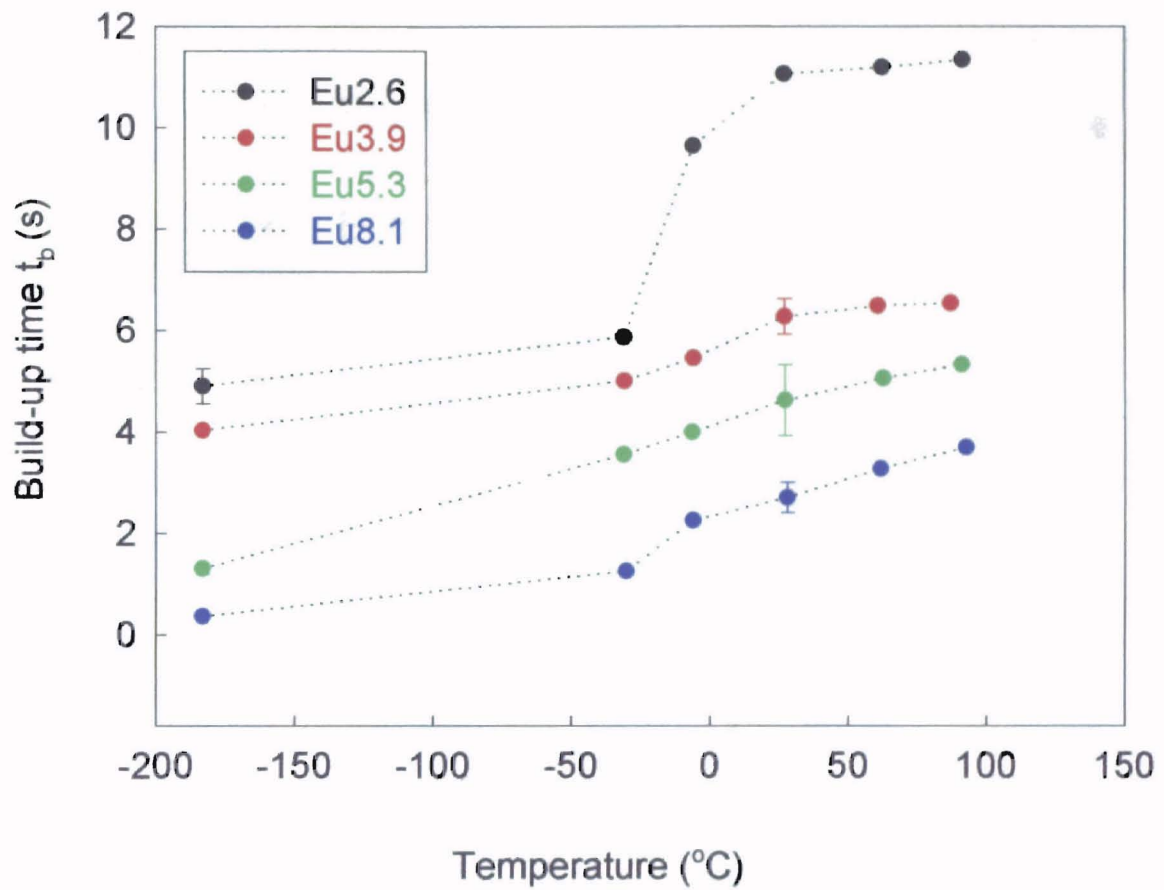
Figure 6. Temperature dependence of build-up time of the maximum grating, Eu2.6, Eu3.9, Eu5.3, Eu8.1, $2\theta_w=5.145^\circ$, $P_w=50mW$
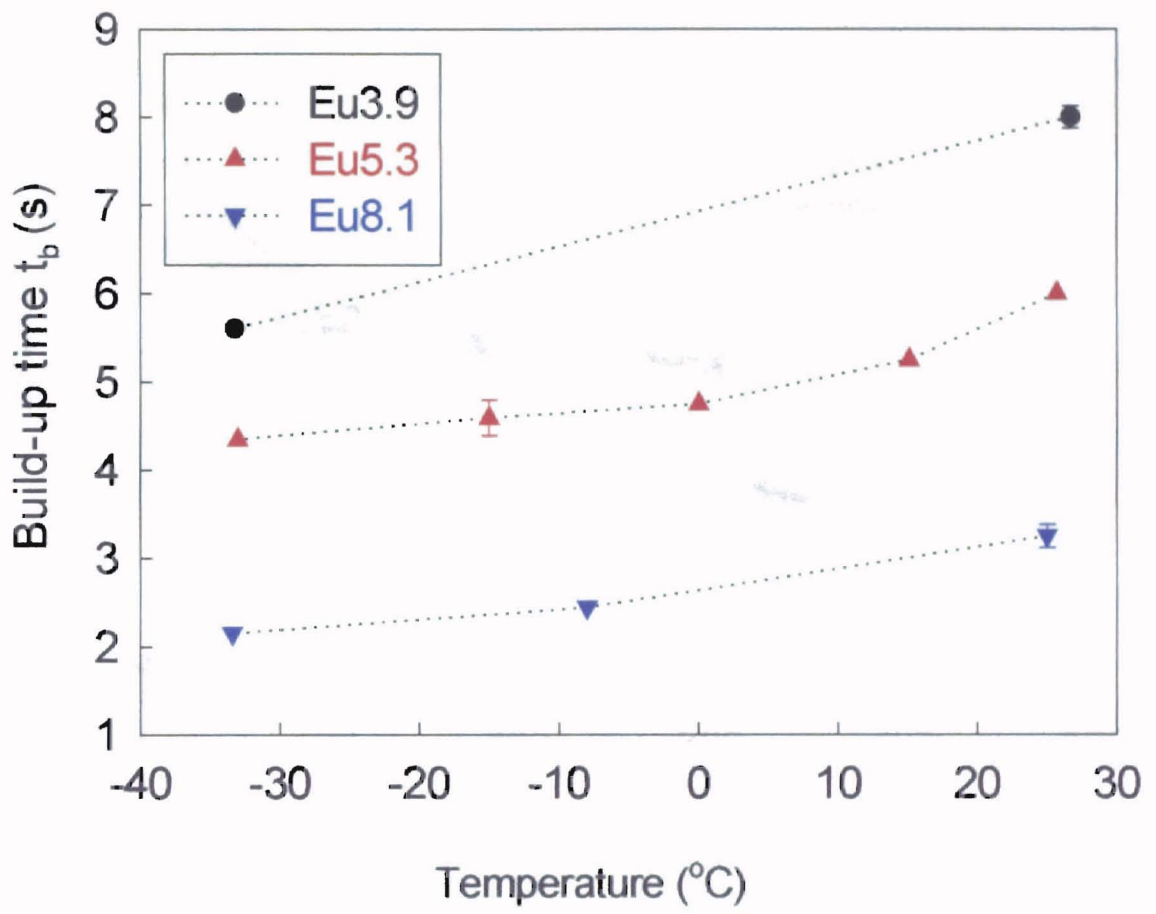
Figure 7. Temperature dependence of build-up time, P_w=50mW, $2\theta_w$=8.75°
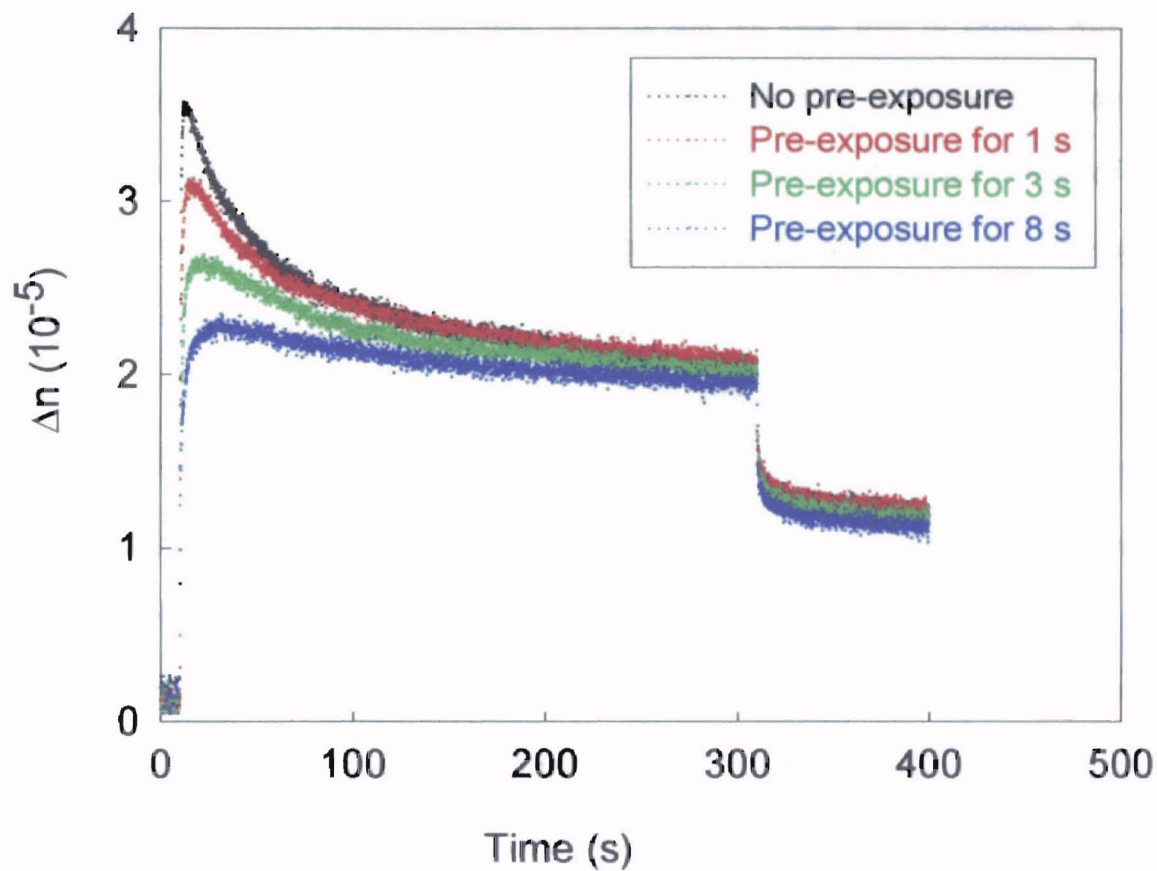
Figure 8. Pre-exposure effect on the grating kinetics for different pre-exposure times at 27 $^{\circ}$C, Eu 3.9, $2\theta_w$=5.145°

As Fig. 2 shows, the diffracted signal begins to decay after the initial maximum. During the process, both write beams are kept on. It is still not clear how to explain why the grating decays after it reaches the maximum. Experiments were performed to study the temperature dependence of the decay process. Figs. 9 and 10 show the results of the persistent decay for the Eu8.1 and Eu5.3 samples at different temperatures of grating formation, which changes from -196°C to 92.7°C. The decay procedure is defined as decay from the maximum of the signal when both write beams are kept on. Due to the difficulty of defining the decay rate quantitatively, the best way is to compare the decay curves directly. Since the change in the index of refraction has different maxima at different temperatures, the curves have been normalized to the maximum of one or one thousand to compare the temperature dependence of the decay rate. All these curves present one trend. That is, as the temperature increases, the decay rate of the persistent grating will decrease.

3.5 Temperature dependence of grating after the write beams are blocked at the maximum:

As Fig. 3 shows, during the experiment process, it was found that the persistent grating decayed if both write beams were blocked at the same time. This occurs after the disappearance of transient grating. Experiments were performed to study how the persistent grating evolves with time at different temperatures after both write beams are blocked. To make the decay process of the persistent grating clear, as soon as the diffracted signal reached the maximum, both write beams were blocked for five minutes. Each curve is normalized by making the maximum change in the index of refraction
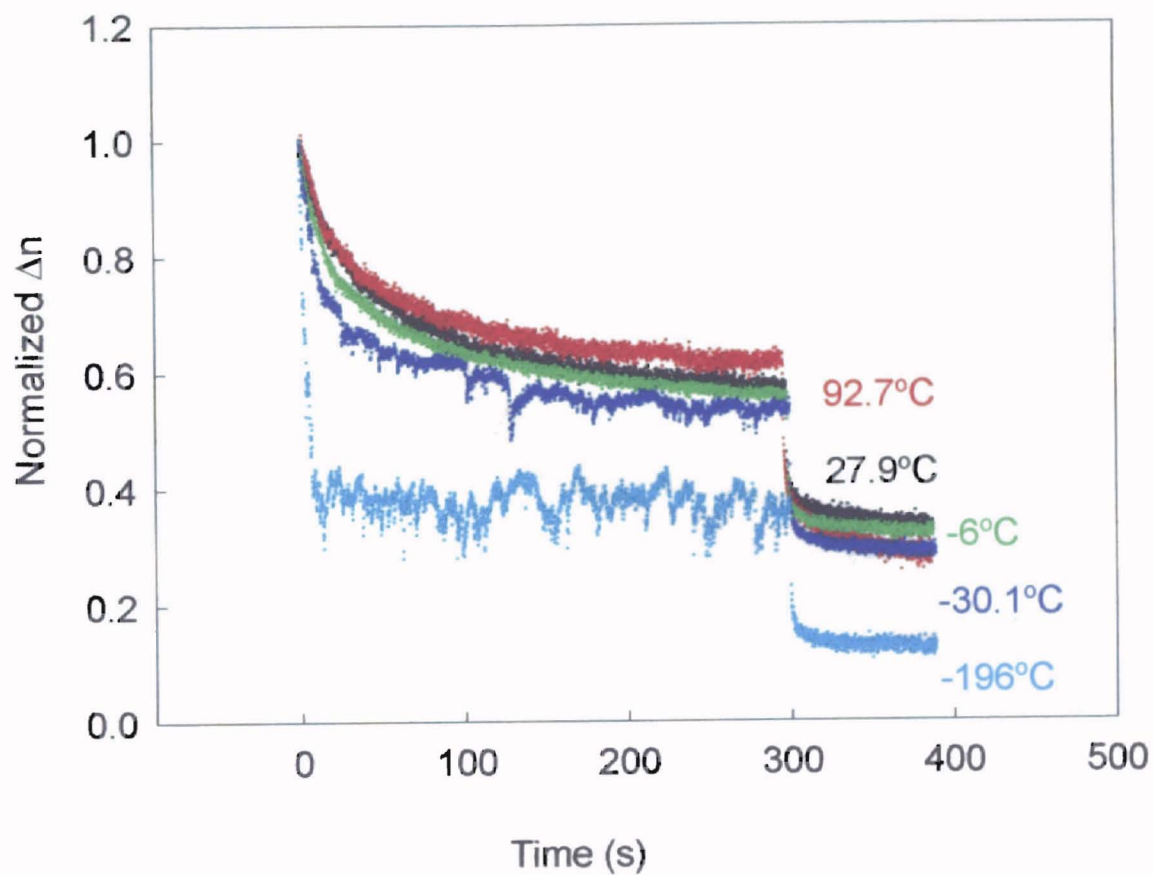
Figure 9. Temperature dependence of the persistent decay while writing, Eu8.1, $2\theta_w = 5.145^\circ$
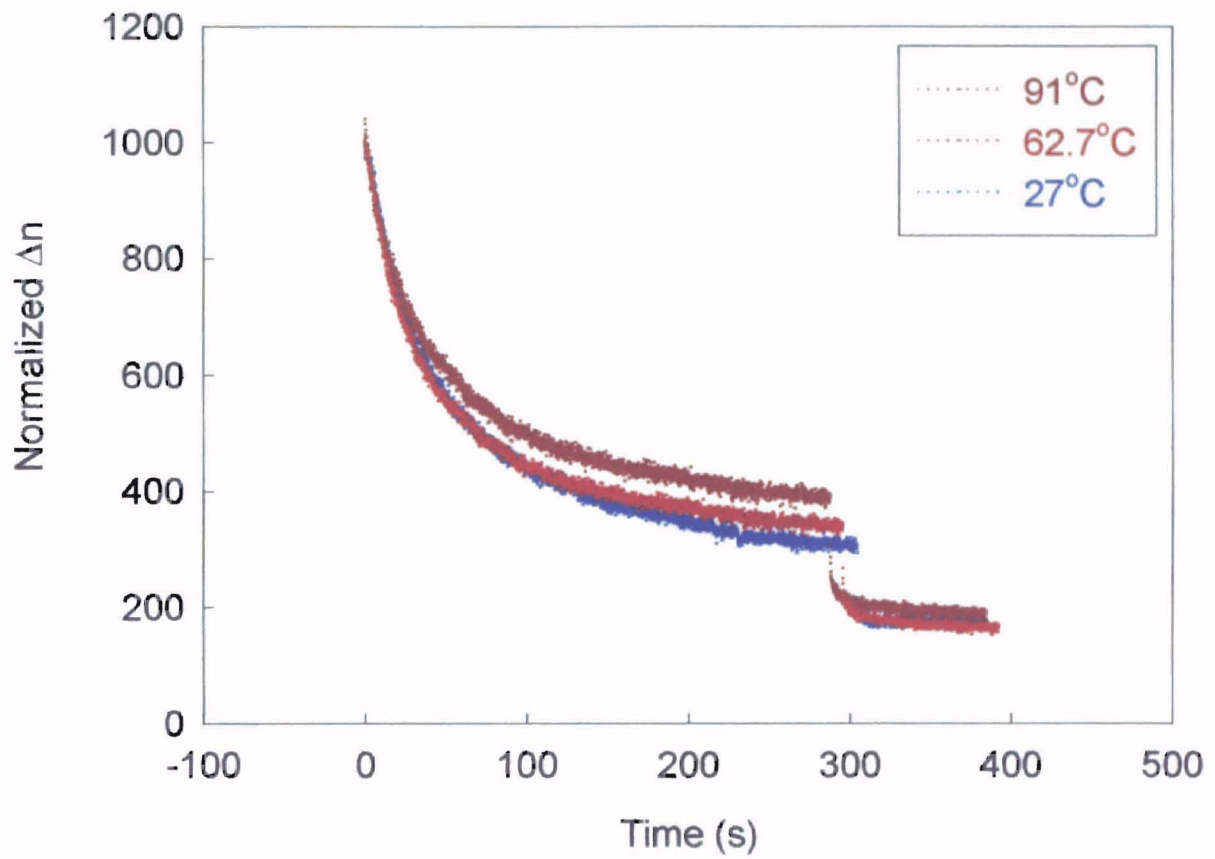
Figure 10. Temperature dependence of the persistent decay while writing, Eu5.3,
$2\theta_w=5.145°$
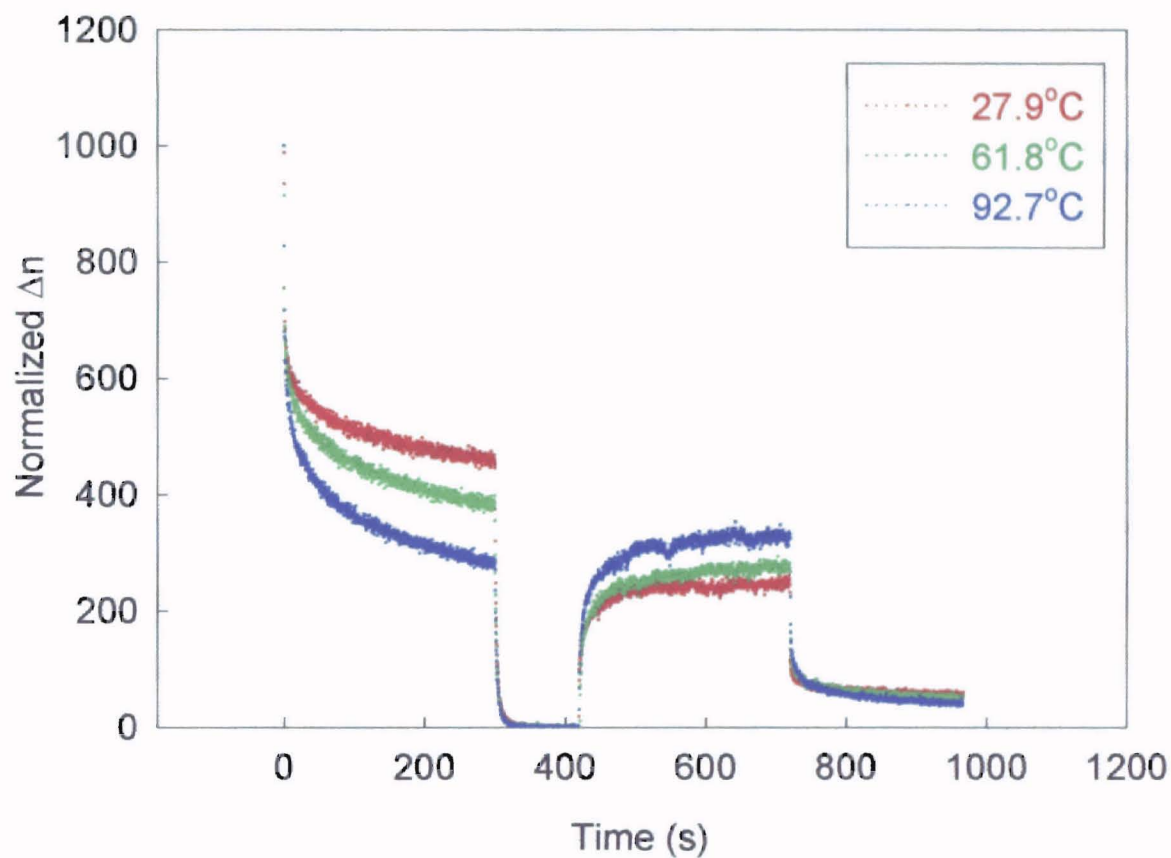
Figure 11. Temperature dependence of the grating blocked at the maximum at different temperatures, Eu8.1, $2\theta_w=5.145^\circ$

equal to 1000. Then one write beam was turned on to erase the grating for two minutes. After that, another write beam was turned on to rewrite the grating. Fig.11 presents the experiment curves for the Eu8.1 sample with the temperature range from 27.9°C to 92.7°C. From these measurements, we see that a more persistent grating is left at higher temperature.

3.6. Temperature dependence of the erasure rate:

As stated earlier, the grating can be erased by a single write beam, so the temperature dependence of the erasure rate is of interest. Fig. 12 shows how the erasure rate changes for the Eu5.3 sample. Every curve is normalized by making the diffracted signal at the beginning of the erasure procedure to one. The measurements for the samples Eu2.6, Eu3.9 and Eu8.1 show similar trends. From Fig. 12, we can see that the erasure rate decreases when the temperature increases.

3.7 Temperature dependence of the rewrite procedure of the grating:

As Fig. 11 shows, after the erasure process lasted for two minutes, another write beam was turned on to regenerate the grating. Fig. 13 presents the rewrite procedures of the grating for the Eu8.1 sample at different temperatures. Experiments were also performed on the samples Eu2.6, Eu3.9 and Eu5.3. We find that a much stronger rewrite grating is achieved at the higher temperatures.
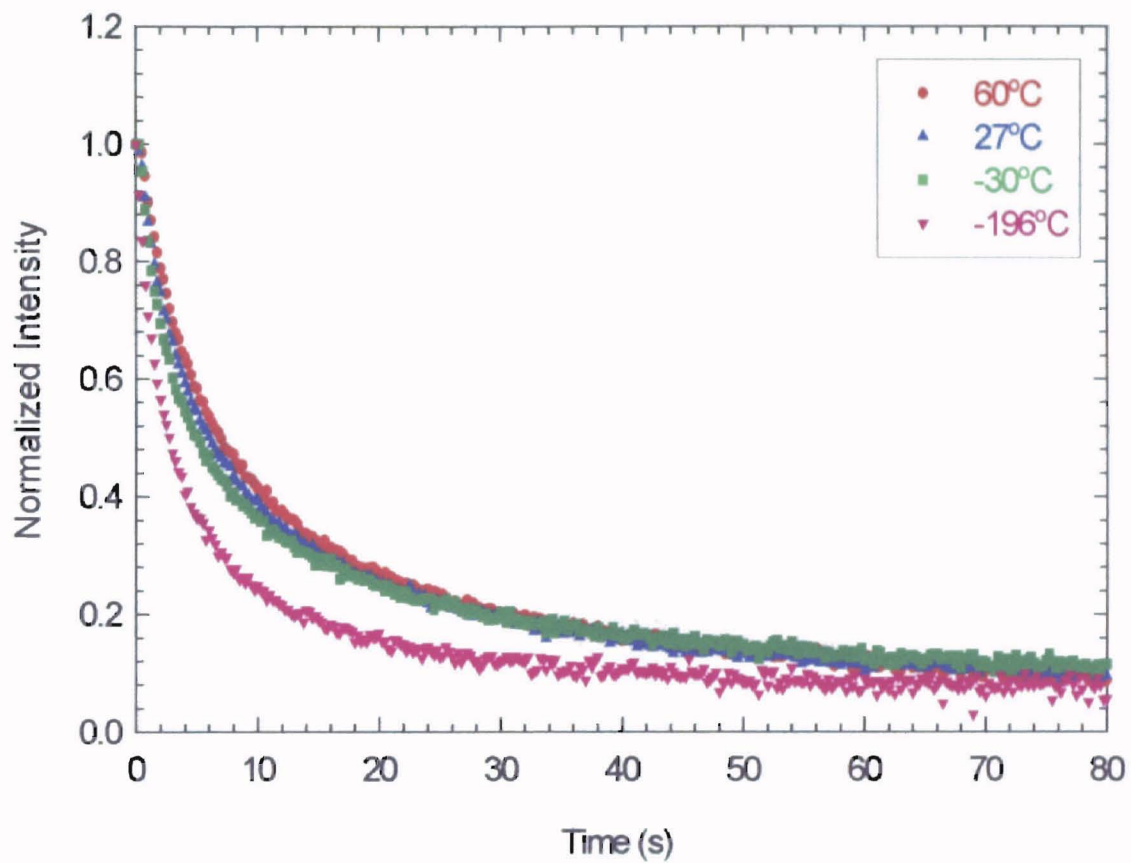
Figure 12. Temperature dependence of erasure of the grating blocked at different temperatures, Eu5.3, $2\theta_w=5.145°$
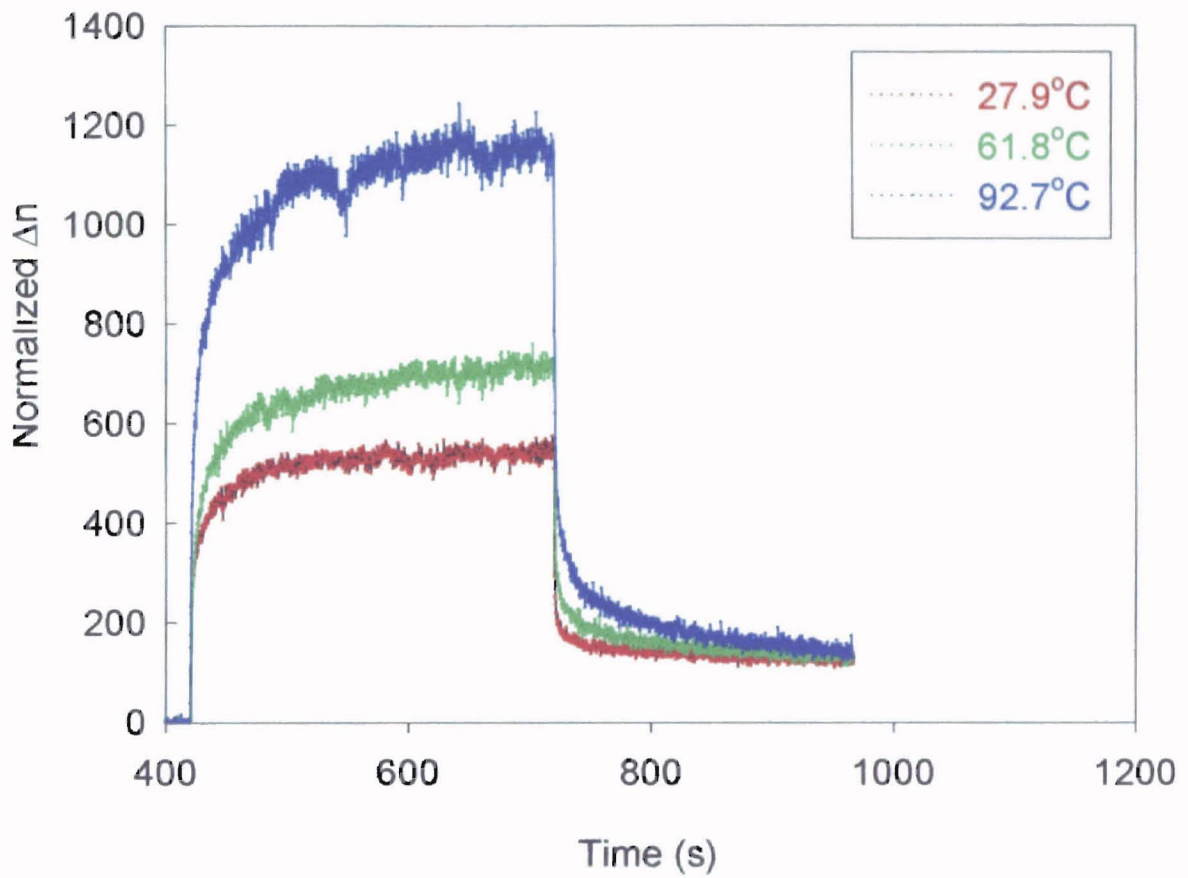
Figure 13. Temperature dependence of rewrite process of the grating at different temperatures, Eu8.1, $2\theta_w = 5.145°$
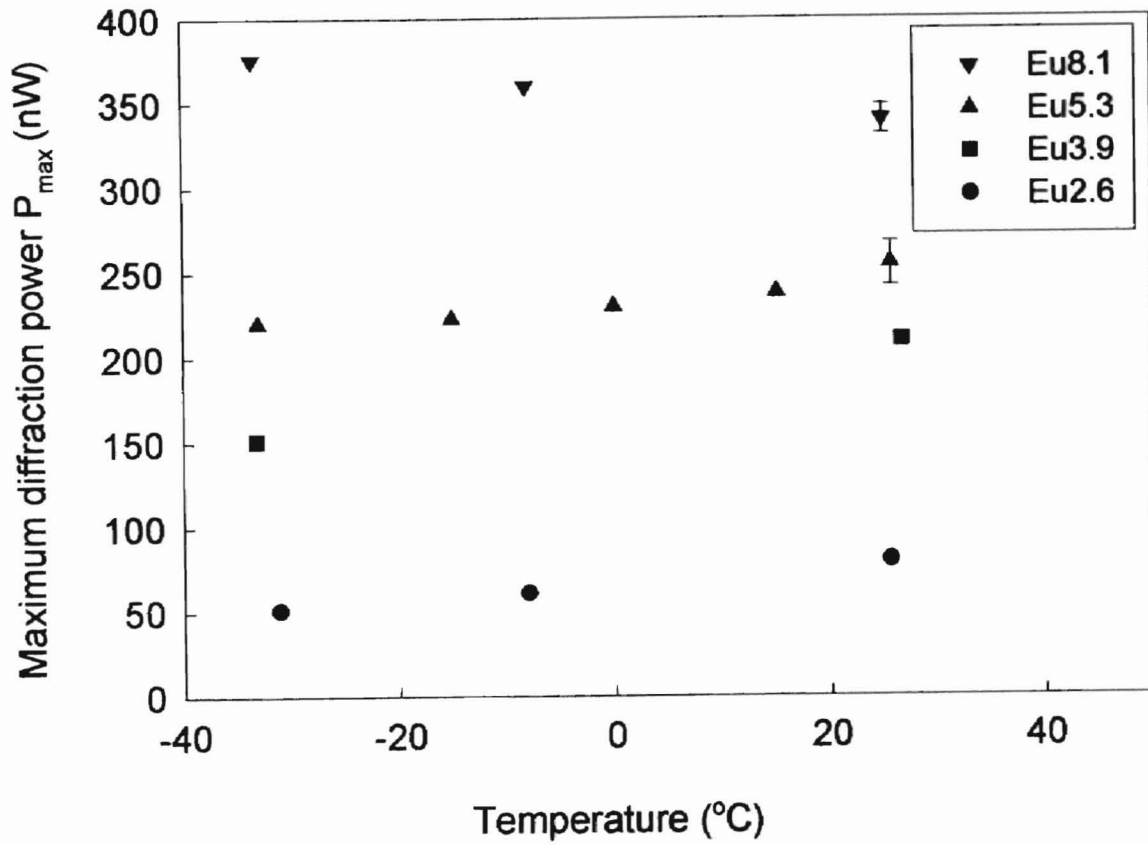
Figure 14. Temperature dependence of maximum diffracted power P_{max} at different temperatures, Eu2.6, Eu3.9, Eu5.3, Eu8.1, $2\theta_w=8.75°$, $P_w=50mW$
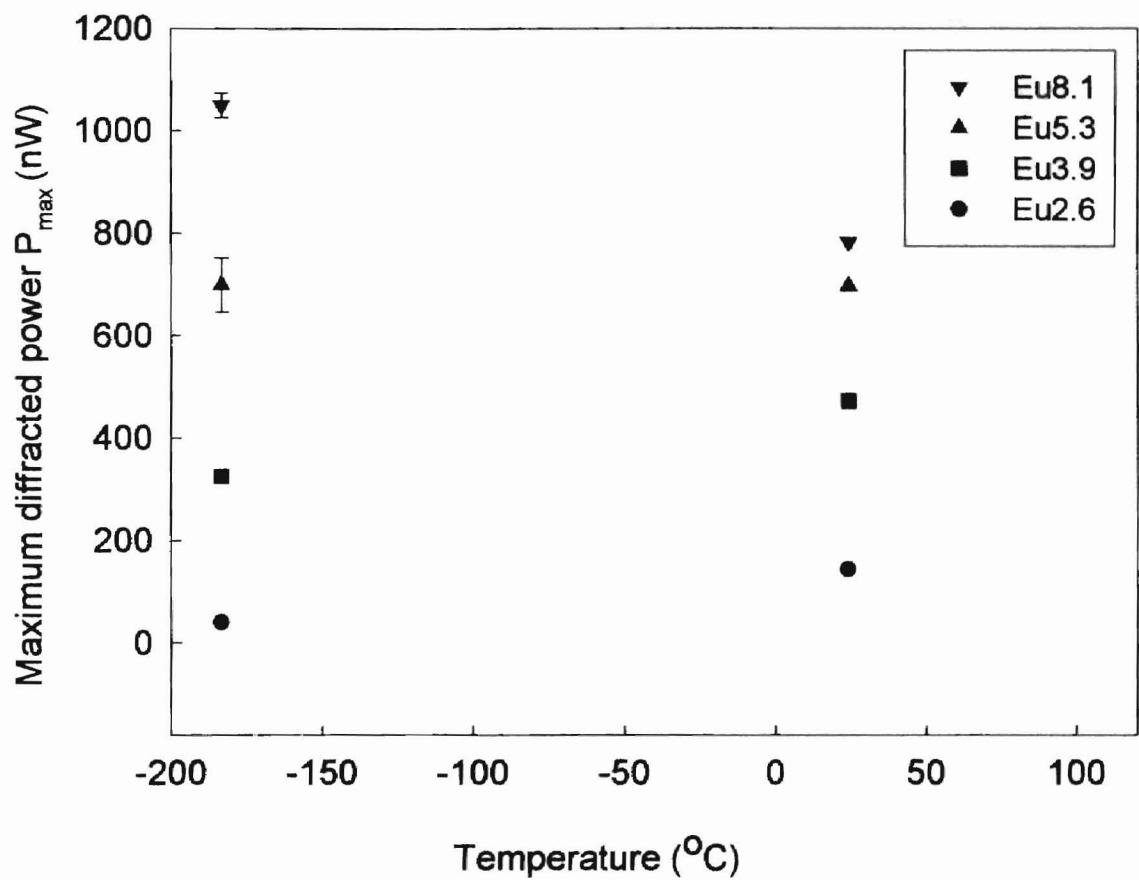
Figure 15. Temperature dependence of maximum diffracted power P_{max} at different temperatures, Eu2.6, Eu3.9, Eu5.3, Eu8.1, $2\theta_w=3.87°$, $P_w=50mW$

3.8 Temperature dependence of the maximum of diffracted signal:

Figs. 14 and 15 show how the initial maximum changed as we lowered the temperature of the samples with a different Eu^{3+} concentrations. The range of temperature is from 27 °C to -33 °C for Fig. 14 and to -196 °C for Fig. 15, respectively. The crossing angles are different in these two figures. For the Eu8.1 sample, the initial maximum increased as the temperature was lowered. For the other samples--Eu2.6, Eu3.9 and Eu5.3, the initial maximum decreased at the lower temperatures. These results are not consistent with the results reported by Behrens *et al.* [13] and French *et al.* [14]. To examine the trends, experiments have been conducted systematically from –196 °C to 93 °C. Figs. 16, 17 and 18 show the result for the samples Eu2.6, Eu3.9, Eu5.3 and Eu8.1 at the crossing angle $2\theta_w = 5.145^0$. Figs. 16, 17 and 18 present the maximum change, the maximum persistent change and the transient change in the index of refraction as a function of temperature respectively. The error bars in Figs. 14, 15 and 16 are the maximum ones of all measurements for each sample respectively. The error bars in Figs. 14 and 15 for the samples Eu2.6 and Eu3.9 are all smaller than their symbol sizes. Error bars are not applicable to the Figs. 17 and 18 since their measurements are conducted for only one time.

3.9 Liquid nitrogen measurements:

As we mentioned before, the experiments have been performed at liquid nitrogen temperature. Figs. 19 and 20 illustrate the typical curves for the Eu2.6 and Eu5.3 samples at the crossing angle $2\theta_w = 5.145^\circ$, respectively. As can be seen from the curve, the signal decayed very fast as soon as it reached the initial diffraction maximum at liquid nitrogen

temperature. An oscillation of the signal is also observed, which is not found at room temperature. This phenomenon is discussed in the next chapter.
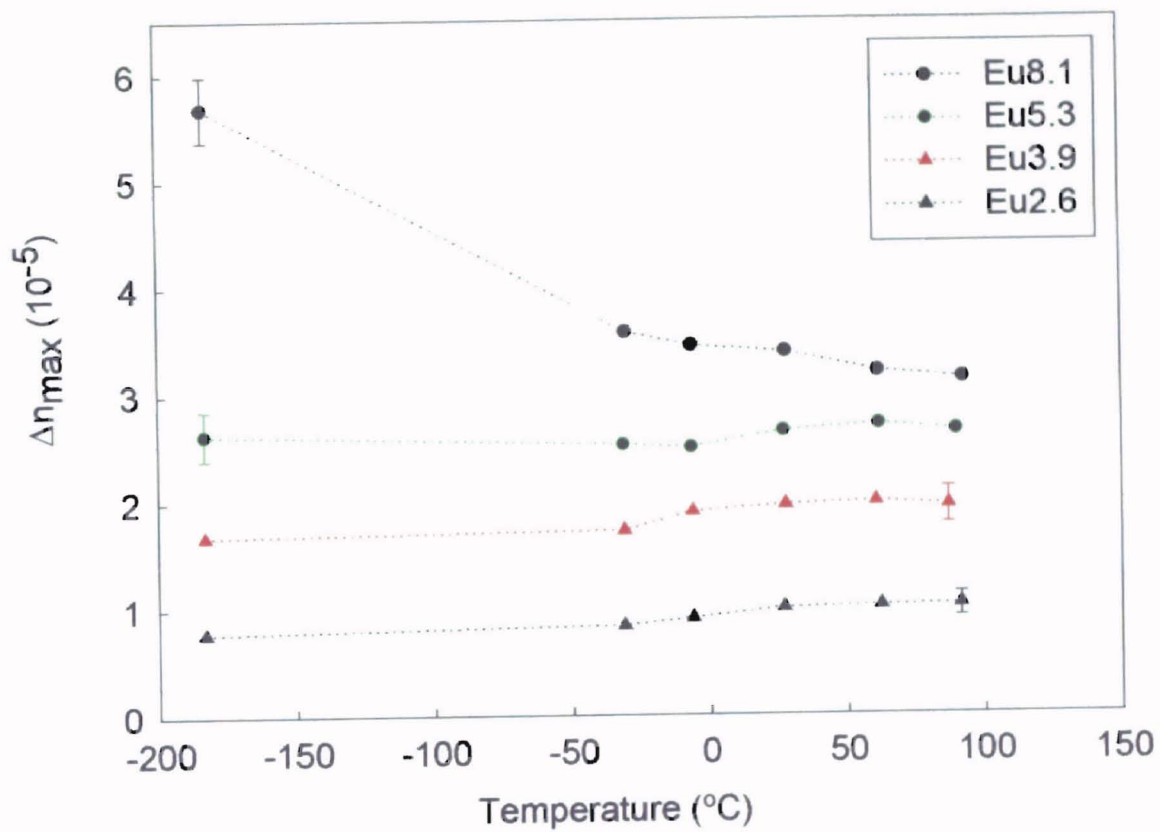
Figure 16. Maximum change in index of refraction as a function of temperature for Eu2.6, Eu3.9, Eu5.3 and Eu8.1
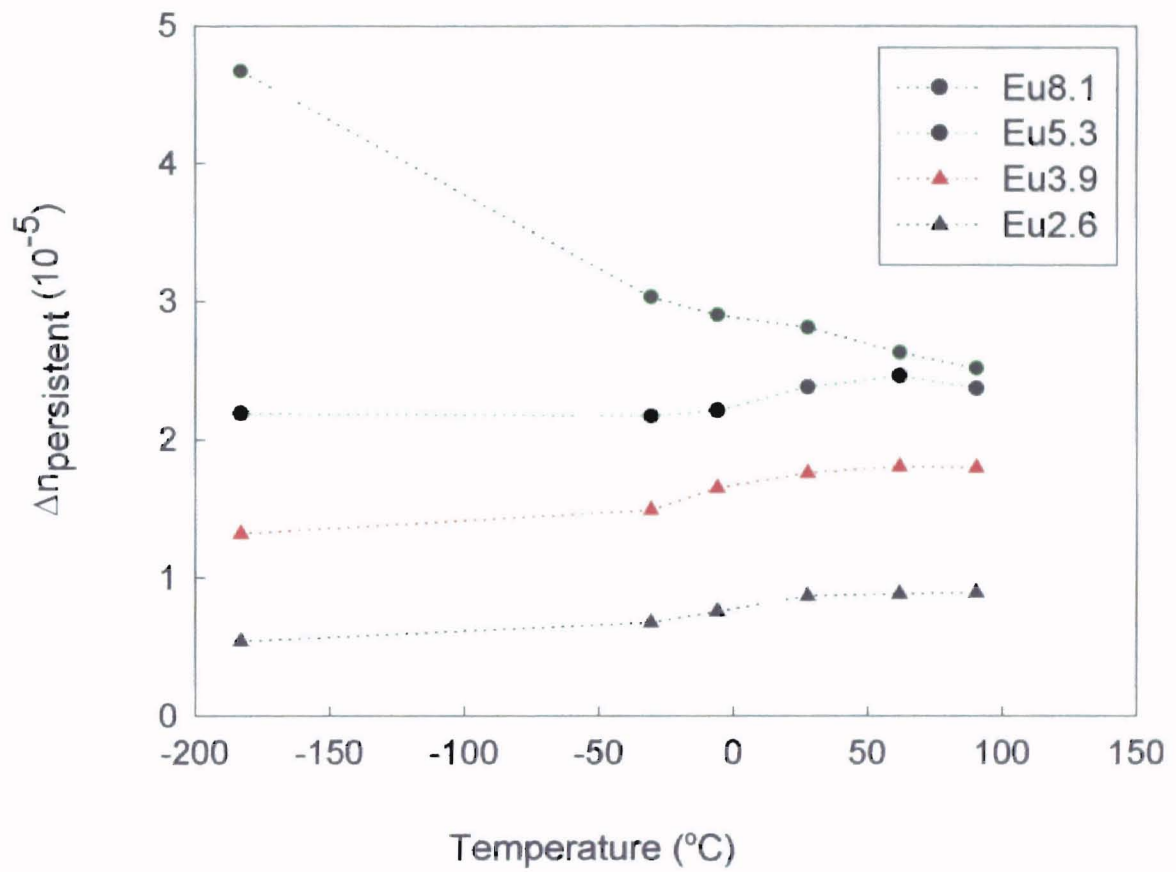
Figure 17. Maximum persistent change in index of refraction as a function
of temperature for Eu2.6, Eu3.9, Eu5.3 and Eu8.1
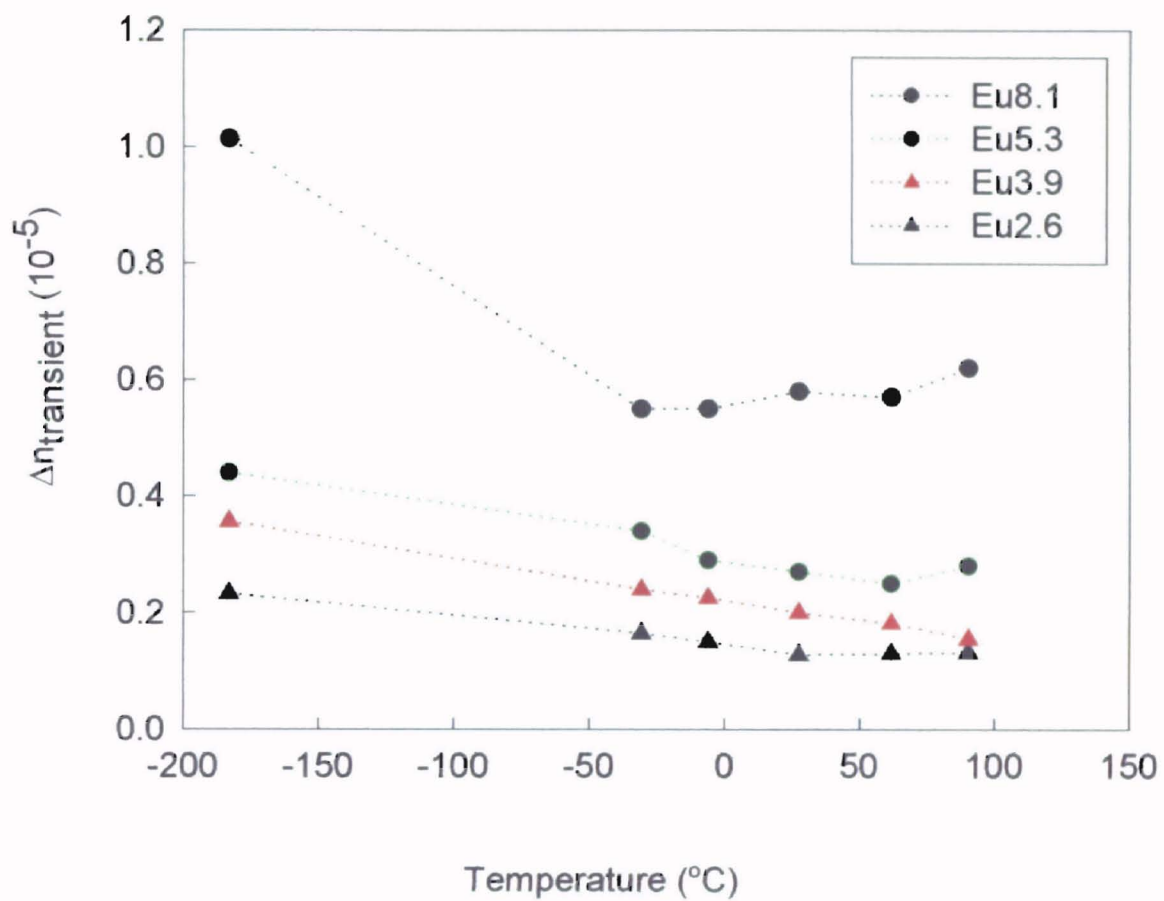
Figure 18. Transient change in index of refraction as a function of
temperature for Eu2.6, Eu3.9, Eu5.3 and Eu8.1
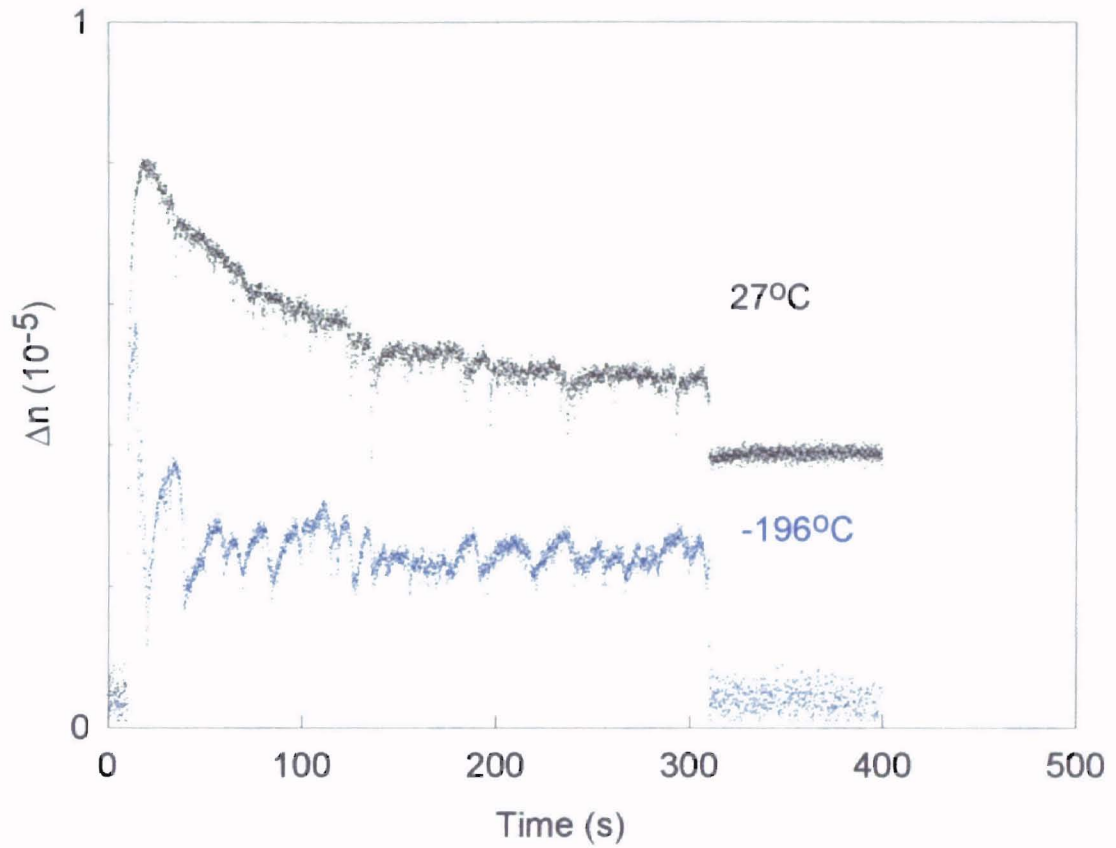
Figure 19. Typical scans of the sample Eu2.6, P_w=50mW, at T=27°C
and -196^oC
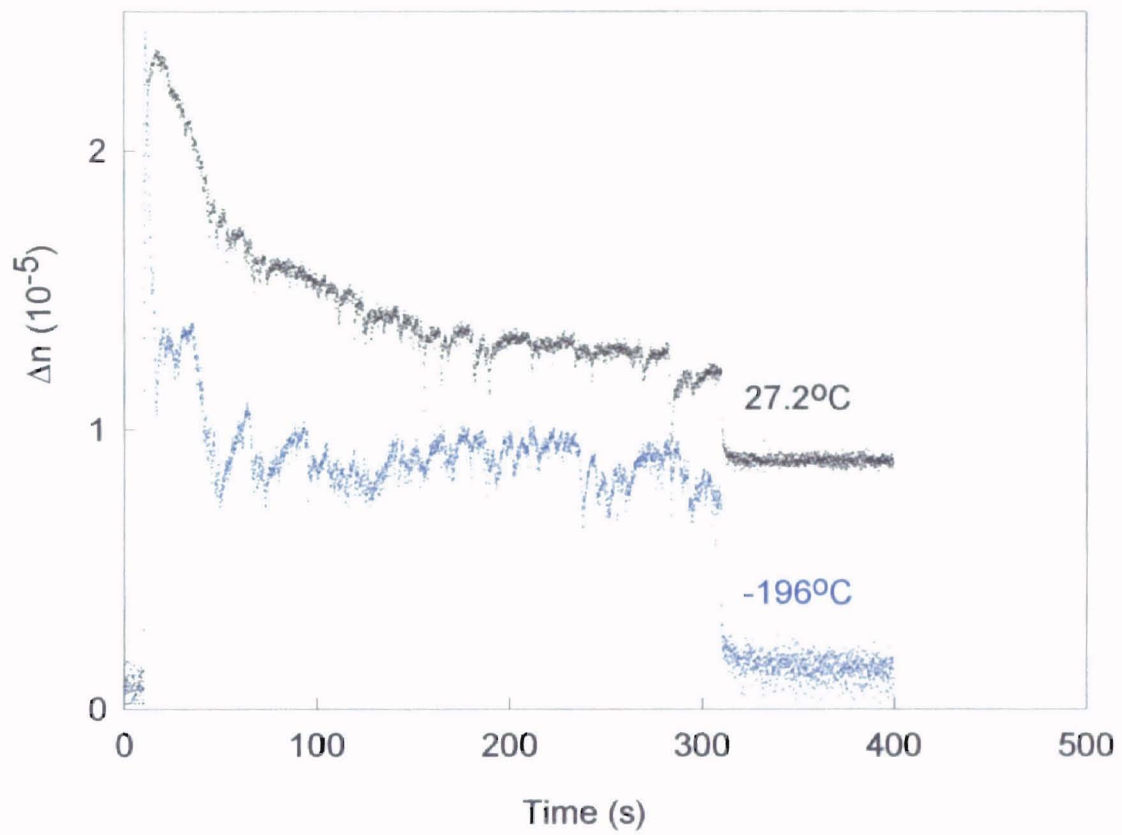
Figure 20. Typical scans of the sample Eu5.3, P_w=50mW, at T=27.2°C
and −196°C

CHAPTER 4

DISCUSSION

4.0 Theoretical model and simulation results:

According to Dixon *et al.* [12], the persistent grating is attributed to a modulation in the concentration of small network modifiers. The refractive index of glasses depends on the concentrations of network modifiers. It can be expressed by the following equation:

$$n_d = \sum_i n_{d,i} c_i / 100$$

The c_i factors are the concentrations of the component oxides in mol%, and the $n_{d,i}$ factors are the corresponding contributions to the refractive index. Before the write beams are turned on, the small net modifiers are distributed inside the samples uniformly. If $M(x,t)$ is used to represent the density of the modifiers, $M(x,t)$ is a constant at the beginning. When both write beams are turned on and the grating is created, the mobile modifiers move from the previous trapping sites to the new sites. The mobile modifiers must be small enough in diameter to pass along the interstices of the network. Thus the light alkali or alkaline earth modifiers, such as Na, Li, and Mg, will be the chemical species that can move efficiently resulting in the formation of persistent gratings. Fig. 21 provides a demonstration of the distribution of the ions and atoms in the glass network. Generally, the modifiers are bound in potential wells, which are due to nonbridging oxygens (NBO's) and AlO_4^-. To be mobile, a modifier must be in a well that is shallow enough to allow the local hot phonons to excite it out of the well. It can be expected that the density of the mobile modifiers is substantially smaller than the total density of the
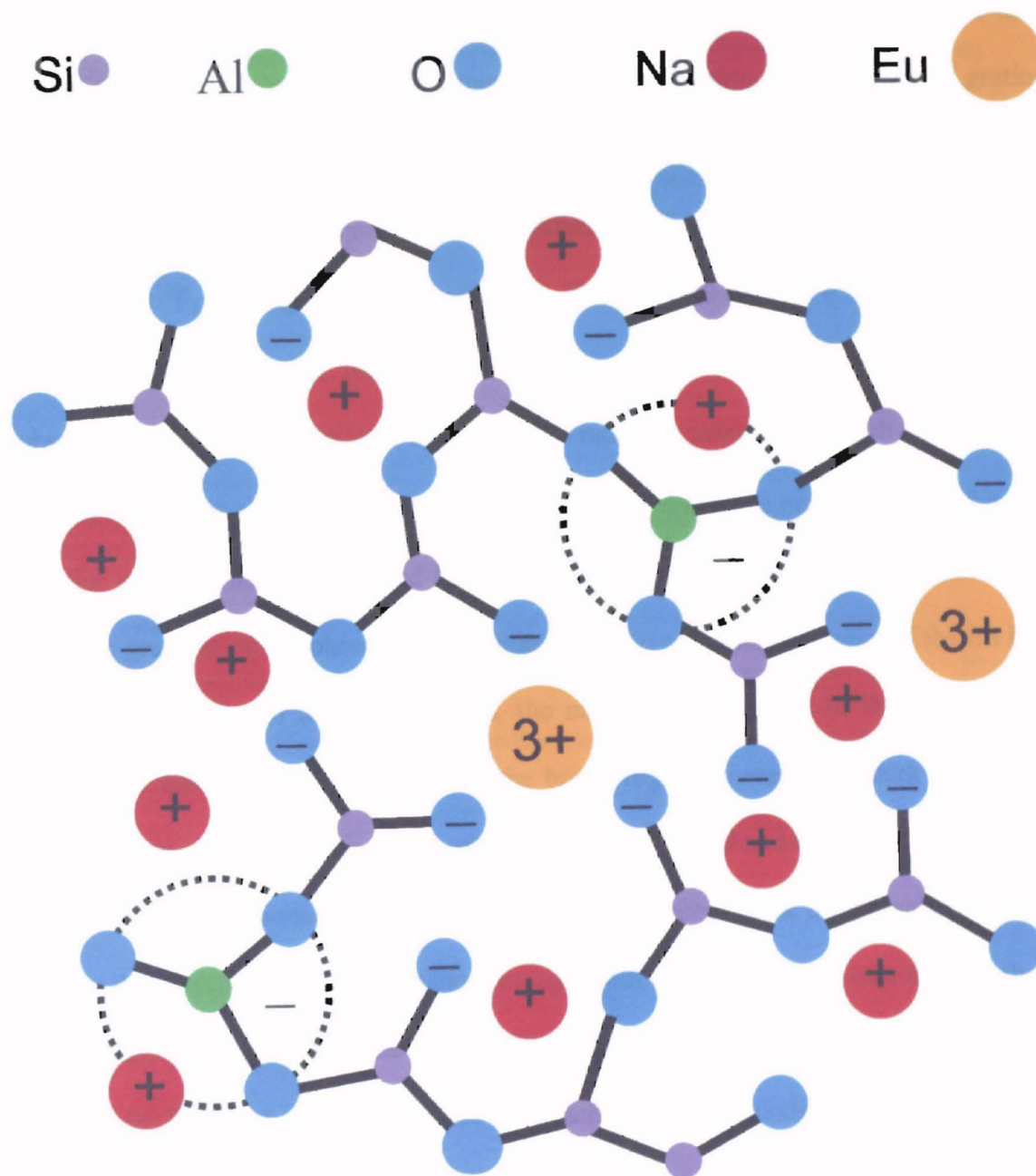
Figure 21. Eu^{3+} environment from Hamad *et al.* [16]

modifiers. According to Behrens *et al.* [4, 5], nonradiative relaxation of the rare-earth excited state creates the hot phonons that drive the production of the persistent grating. Fig. 22 shows the Eu^{3+} energy diagram. For the Eu^{3+} ions that have been excited to the upper electronic state $^5D_2$, there are two possibilities. First is that they drop back to the ground state ^7F_J through radiative relaxation. This process of $^5D_2 \rightarrow ^7F_J$ doesn't happen efficiently. Second is that they relax nonradiatively to the lower excited states and subsequently relax to the ground state through radiative relaxation, which are $^5D_0 \rightarrow ^7F_J$ and $^5D_1 \rightarrow ^7F_J$. For simplicity, Dixon *et al.* [12] assumed there is only one kind of mobile modifier with the mean density of M_0. Due to the Gaussian profile of the write beam, there is a gradient of hot phonons that results from the nonradiative decay of the Eu ions. Under the influence of the hot phonons, the mobile ions can hop to their neighboring sites, which means they can move from the bright regions towards the dark regions. At the same time, drift under the action of the space-charge field and external electric field is also considered in the model. Since the glass contains sites where the potential wells are so deep that the mobile modifiers cannot escape from them once these ions fall into them, Dixon *et al.* [12] considered the effect of these trapping sites. Finally, the full transport equation by Dixon *et al.* [12] included all possible effects including diffusion, drift and deep traps. We need to keep in mind that these equations are based on a one-dimensional diffusion model, which is a simplification of the actual three-dimensional case.

The transport and trapping equations were reduced to a following set of coupled rate equations [12]:

$^5D_2$

← Multi-phonon emission

$^5D_1$

$^5D_0$

454-488 nm

520-560 nm

580-640 nm

$^7F_2$

$^7F_1$

$^7F_0$
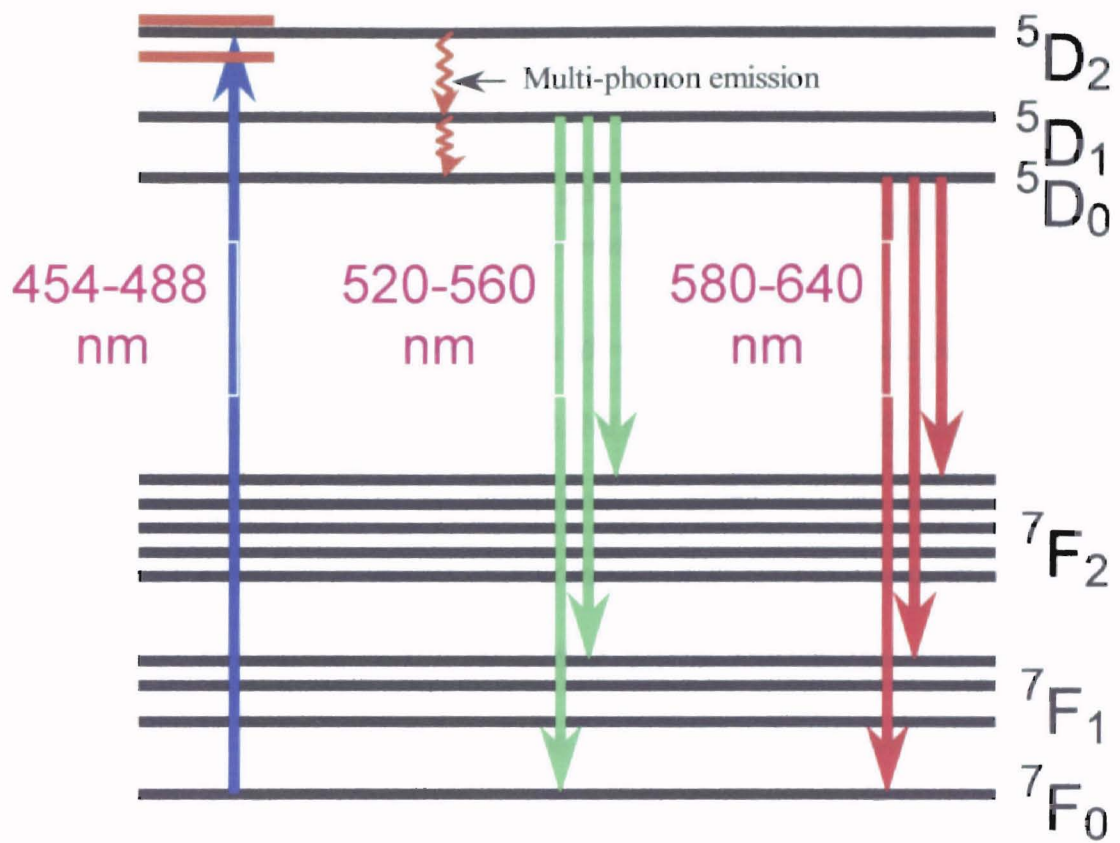
Figure 22. Eu^{3+} energy diagram from Hamad *et al.* [16]

$$\dot{M}_n + \dot{N}_n = -\beta_n \left(2M_n + mM_{n+1} + mM_{n-1} \right) \quad (22)$$

and

$$\dot{N}_n = \gamma_T \phi_0 S_T \left(2M_n + mM_{n+1} + mM_{n-1} \right)$$
$$- \gamma_T \phi_0 \sum_p N_p \left(2M_{n-p} + mM_{n-p+1} + mM_{n-p-1} \right) \quad (23)$$

where $\beta_n = \gamma_0 \phi_0 S K^2 a^2 n^2 / 2 = n^2 \beta_1$ and $\beta_1 = \gamma_0 \phi_0 S K^2 a^2 / 2$. M_n and N_n are the spatial Fourier coefficients for $M(x, t)$ and $N(x,t)$. $M(x,t)$ and $N(x,t)$ are the densities of mobile modifiers and trapped modifiers respectively. S is the uniform density of sites for modifiers and S_T is the density of traps (a subset of S). a is the mean distance between sites and K is the wavenumber of the grating. T is the temperature of the sample. γ_T is the rate constant for the trapping. γ_0 is the proportional constant between the rate parameter for hopping $\gamma(x,t)$ and the local hot phonon density $\phi(x, t)$. ϕ_0 is the local hot phonon density under conditions of uniform illumination. These equations describe both writing conditions by $m \approx 1$ and optical erasure by $m=0$.

According to Dixon *et al.* [12], the equation (22) comes from diffusion and the equation (23) is due to the effect of trapping. These rate equations describe both the writing of the grating and the optical erasure (bleaching). Optical erasure is done by blocking one of the write beams. The experimental signal is attributed to the first order Bragg diffraction from the persistent grating, which is due to the (M_1+N_1) Fourier amplitude. Because these coupled rate equations represented by (22) and (23) can be solved numerically, the experimental data can be compared with their predictions.

The fits of the experimental data are used to extract the model parameters. β_1 is adjusted to fit the leading edge, which determines the build-up rate of the persistent grating. M_0 is adjusted to fit the initial maximum, which determines the intensity of the persistent grating. $\gamma_T \phi_0 S_T$ is adjusted to fit the decay of the grating, which determines the decay rate of the grating with both write beams turned on. All fits of the model to data were done by successive approximations of those fitting parameters. Figs. 23 and 24 show the fitting curve for the Eu3.9 sample at room temperature. The fitting procedure is divided into three steps. First, from the experimental data presented by Fig. 24, the intensity of the transient grating was obtained, and it was applied to the fitting of Fig. 23. Second, from the experimental data presented by Fig. 23, the parameters of the model were adjusted to fit the curves. Third, those parameters were applied to the fitting of Fig. 24 and adjusted again to fit the experimental data plus another parameter for the erasure procedure. As stated before, the blocking process lasted five minutes, and the persistent grating decayed during this period of time with both write beams turned off. The theoretical model does not consider how the persistent grating evolves after both write beams are turned off. It means the change in the index of refraction is just a constant during this period and that is not consistent with the experimental data. Hamad *et al.* [16] reported that the grating still existed after twenty months with both write beams turned off. So to resolve this problem, the starting point of the erasure procedure has been shifted to fit the actual persistent change in the index of refraction. The same fitting procedure has been repeated for the same sample at -33°C and 92°C. The fitting parameters are given in Table 2.
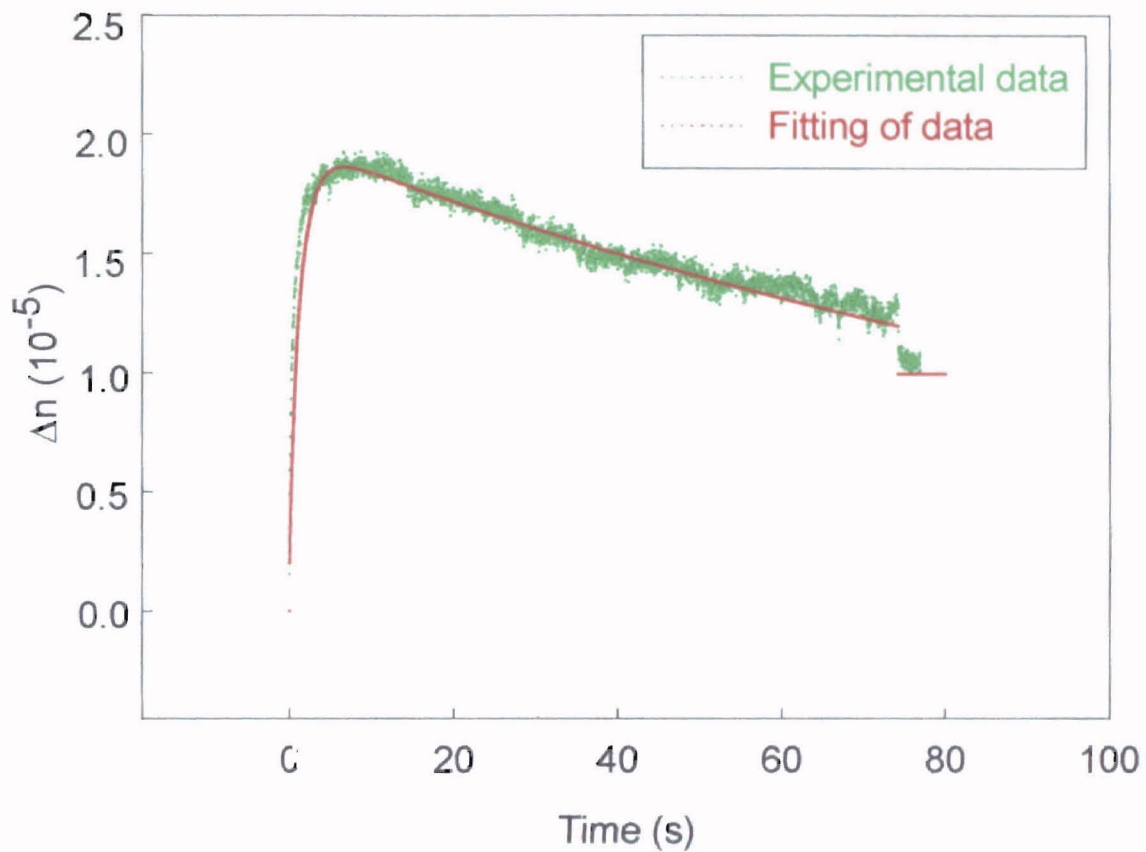
Figure 23. Experimental data and fitting using a Quattro Pro program from Dixon
et al. [12], Eu3.9, T=27°C, $2\theta_w$=5.145°
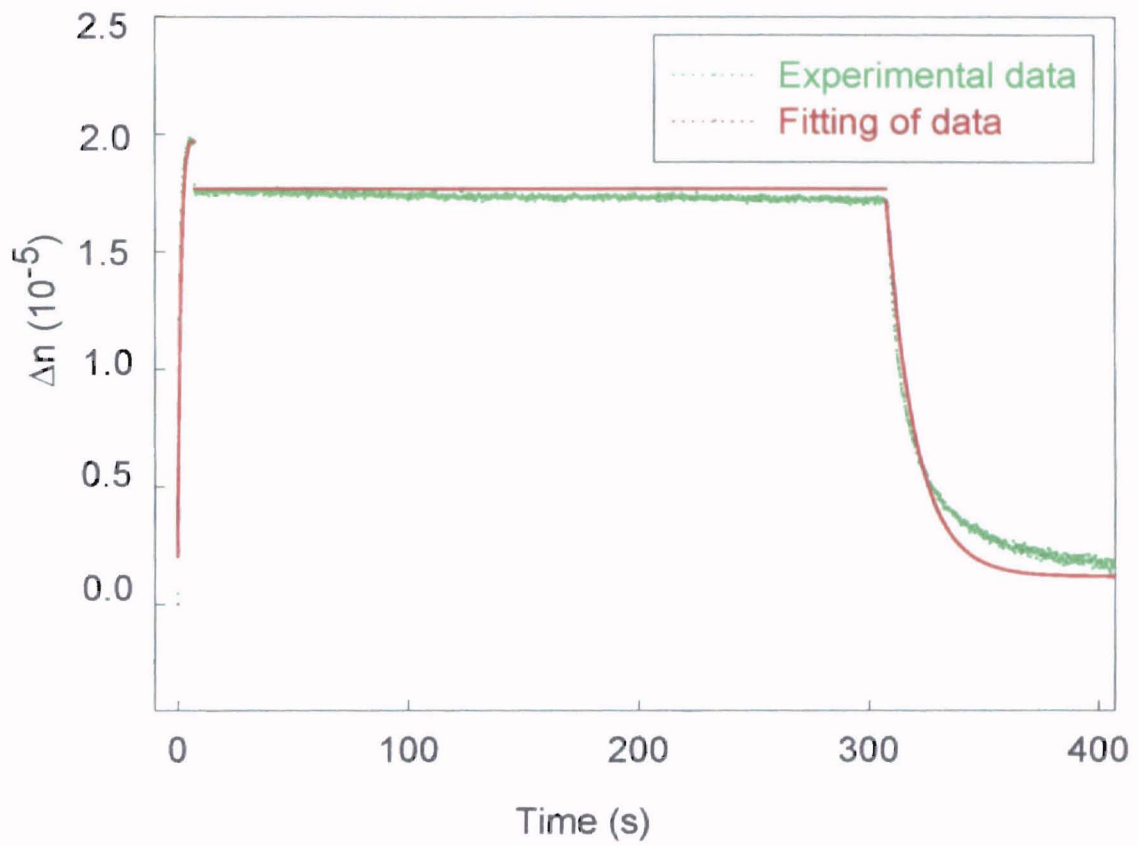
Figure 24. Experimental data and fitting using a Quattro Pro program from Dixon *et al.* [12], Eu3.9, T=27°C, $2\theta_w=5.145°$

Temperature (^{o}C)	β_1 (s^{-1})	M_0 ($10^{20}m^{-3}$)	$\gamma_T\phi_o S_T$ (10^{-4})	$\Delta n_{transient}$ (10^{-6})
-30	1.15	4.83	2.70	2.37
27	0.74	6.00	2.16	2.00
87	0.63	6.13	2.05	1.55

Table. 2. Fitting parameters for different temperatures using the sample Eu3.9, $2\theta_w=5.145^{o}$

From Table 2, it can be seen that the M_0 decreases as the temperature decreases. In contrast, the other parameters all increase at the lower temperature. To understand the physical mechanism behind this process, we need to note how the density of hot phonons and density of trapping sites change with the temperature. According to the absorption experimental results presented by Houck [18], the density of electrons in the ground state $^7F_0$ of the Eu ions increases as the temperature decreases. So there is more absorption to the excited state $^5D_2$ for Eu^{3+} ions from $^7F_0$. The fluorescence data presented by Rahman [19] shows that the intensity of non-radiative decay from $^5D_2$ to $^5D_0$ also increases as the temperature decreases. Because both processes contribute to the production of the hot phonons, the density of hot phonons in the sample can be expected to increase as the temperature decreases. Because the model assumes that the mobile modifiers migrate under the driving of hot phonons, it can be expected that more hot phonons lead more modifiers to move, but there is a conflict with the fact that the density of mobile modifiers decreases as the temperature decreases. However, another factor needs to be considered, which is the density of trapping sites. Table 2 shows that $\gamma_T \phi_0 S_T$ increases as the temperature decreases. To see how the density of trapping sites changes with the temperature, we need to compare different experimental curves at different temperatures. Fig. 25 presents a comparison for the Eu8.1 sample at the crossing angle $2\theta_w=5.145^0$. After the initial maximum, the change in the index of refraction began to decay. The write beams were then blocked. As seen from the curves, as the temperature decreases, there is a less persistent grating although higher initial maximum is obtained. From this, it can be concluded that more shallow traps become deep traps and there are more trapping sites as the temperature decreases. From the point of view of the average trapping

44

potential wells, it can be expected that it increases at the low temperature since there are more deep traps now. That leads to less persistent grating. We need to note the average depth of the potential wells where the mobile modifiers reside. Physically, they are the same as the trapping sites. So, at the trapping sites, their depth increases at lower temperatures, and fewer mobile modifiers might exist at the low temperature. Therefore, there is a competition among these factors, which are the densities of hot phonons and trapping sites. For different samples with different concentrations of Eu ions, the relative effect of these factors might be different.

4.1 Power dependence of grating growth rate:

The data presented in Figs. 4 and 5 show linear dependence of grating formation for Eu3.9 for different crossing angle at low temperatures. The starting point of the model [12] is that the rate of mobile ions hopping between adjacent sites $\gamma(x,t)$ is proportional to the density of the local hot phonons $\phi(x,t)$. It can be written *as $\gamma(x,t) = \gamma_0 \phi(x,t)$*. By a series of successive steps, equations 22 and 23 in the reference [12] are achieved. From them, it can be seen that the transport and trapping coefficients are proportional to the hot phonon density ϕ_0. If the signal build-up rate is measured by the reciprocal of the time that it takes the diffracted signal to reach one-half the initial maximum of the signal intensity [12], it can be expected that the rate of persistent grating is proportional to the power of the write beams. This kind of linear dependence has been indicated by Dixon *et al.* [12] for the sample with 5% Eu concentration at room temperature with $2\theta_w = 4.25^0$, which provides evidence for the assumption of the linear driving mechanism at room temperature. The linear dependence shown in Figs. 4 and 5 confirms the validity of this
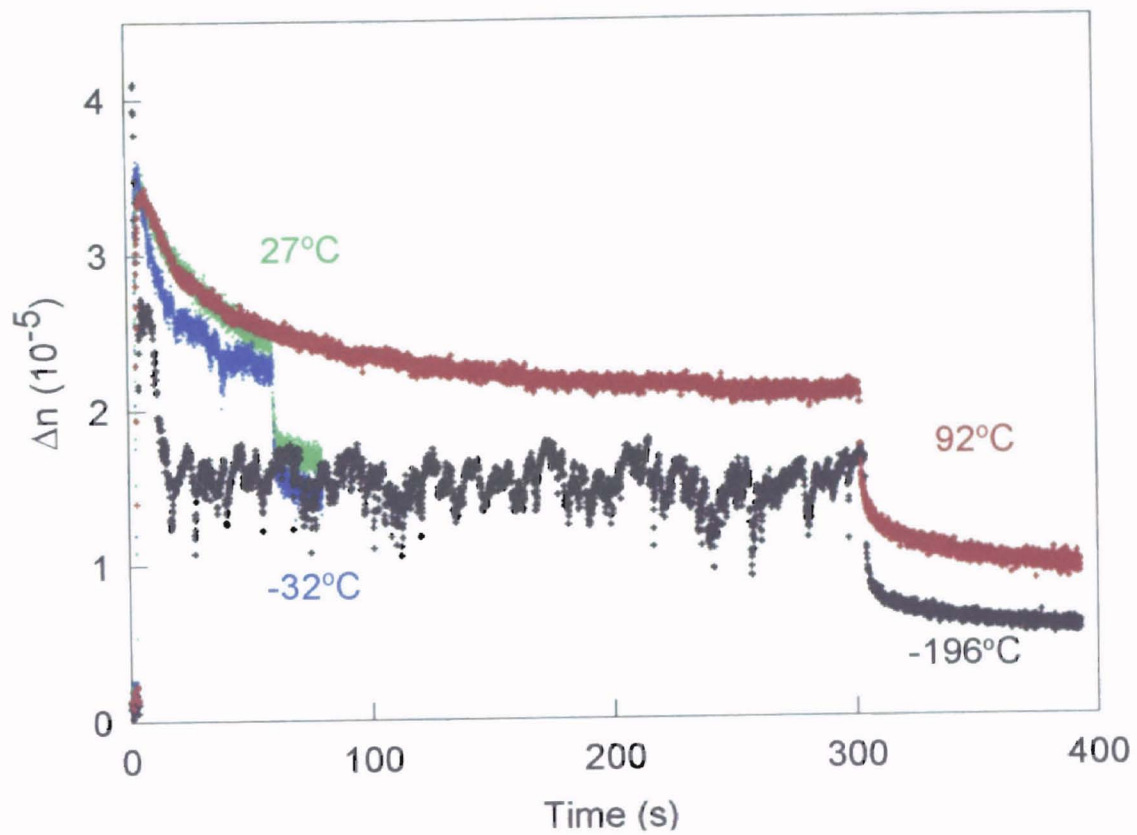
Figure 25. Evolutions of grating intensity of the Eu8.1 sample at different temperatures

assumption for the Eu3.9 sample at -33°C with $2\theta_w=8.75^0$ and for the Eu8.1 sample at -196°C $2\theta_w=3.87^0$. Figs. 4 and 5 show that it is possible to apply the small modifier diffusion model not only to the room temperature but also to other temperatures.

4.2 Temperature dependence of build-up time:

According to the curves presented in Figs. 6 and 7, the build-up time increases when the grating formation temperature increases. The model suggested by Dixon *et al.* [12] attributes the persistent grating to the diffusion and redistribution of the mobile modifiers from the bright regions towards the dark regions, and the build-up rate is proportional to the density of the hot phonons. And at the same time, it can be expected that the ability of the mobile modifiers to move also determines how much time it takes for the change in the refractive index Δn to reach its maximum Δn_{max}. As the temperature decreases, there are more electrons in the ground state for Eu ions. Because of this, the absorption to the $^5D_2$ level increases, which causes an increase in the density of hot phonons. This increases the build-up rate and decreases the build-up time when the temperature decreases. In addition, there is another possible reason. Since there are many collisions between the mobile modifiers and the vibrating glass atoms in the glass network when they move, the intensity of these kinds of collisions will influence the movement of the modifiers. The vibration of the glass atoms can be thought of the phonons with different frequencies. According to Kittel [17], the average number of the phonons with the frequency w can be expressed as

$$< n >= \frac{1}{\exp(hw/K_bT)-1}.$$

So there are fewer thermal phonons when the temperature decreases. It can be expected that fewer collisions will occur and it is easier for the mobile modifiers to move to new sites at the lower temperature. Thus, the build-up time will be smaller and the build-up rate will be larger as the temperature decreases, which is exactly the trend the results indicate.

4.3 Pre-exposure effects:

As Fig. 8 shows, the initial maximum of the signal can be lowered if a fresh spot in the sample is exposed to a single write beam for a certain time period and then another write beam is turned on to write the grating. If the time for which the single write beam is kept on is defined as the pre-exposure time, then a smaller signal maximum is achieved as the pre-exposure time increases. To explain this phenomenon, we need to keep in mind that the mobile modifiers are bound to the potential wells with different depths. Some of these are deep, which could be the case if the mobile ions are bound to the non-bridging oxygens as shown in Fig. 21. Some of these are shallow, which could be true if the ions are bound to the Al complexes, both with tetrahedral and octahedral coordinates. If the sample is warmed to 530 °C for four hours, the modifiers will distribute uniformly inside the sample and remove any memory of a previous grating. In fact, this is the method that we use to erase the grating that had been previously written in the sample. After the sample is annealed from 530 °C to room temperature, it can be expected that the modifiers are bound to the potential wells with different depths. The modifiers bound to

the deep potential wells have a low possibility of moving. In contrast, the modifiers bound to the shallow potential wells have a high possibility of moving when hot phonons are provided. According to Kittel [17], the possibility for the ions to hop from the potential wells is proportional to $exp(-E/K_bT)$, where E is the depth of the potential well, K_b is the Boltzmann constant and T is the temperature. From this, it is clear that the deep potential wells correspond to low possibilities for bound modifiers to hop out of these potentials. When a single beam is used to expose a fresh spot in the sample, it can provide the source of hot phonons. These hot phonons can excite the mobile modifiers out of the shallow potential wells, and later some of these fall into the deep potential wells. It is difficult for them to move out of those deep potential wells again due to their large depths. The longer pre-exposure time results in more modifiers in shallow potential wells migrating to the deep potential wells. When both write beams are turned on to write the grating, it is difficult for these modifiers to move again because they are trapped within the deep potential wells. This can explain why the maximum is lowered as illustrated in Fig. 8. However, there is another possible reason for this phenomenon. In the model of Dixon *et al.* [12], both write beams are assumed to be plane waves, which have uniform profiles. But, in fact, both write beams have Gaussian profiles. Due to the Gaussian profile of the pre-exposure write beam, it can be expected that the density of the generated hot phonons displays a similar Gaussian profile. So a gradient of the density of hot phonons exists. It can be expected that the mobile modifiers move away from the center of the focused laser beam within the glass to the edge due to this gradient. Some of these become trapped in shallow wells, while others are trapped in the deep potential wells. Both reasons produce the same result that the density of mobile modifiers inside

the spot is lowered due to the pre-exposure and less grating intensity is achieved when the second write beam is turned on to generate the grating. It can also be expected that a longer pre-exposure time leads to a smaller maximum of the grating intensity.

4.4 Temperature dependence of decay rate:

Figs. 9 and 10 show the results of the decay curve for the Eu8.1 and 5.3 samples at different temperatures. Both figures indicate one trend. As the temperature decreases, the decay rate will increase. For the Eu2.6 and Eu3.9 samples, there is the same trend. This trend can be explained by the previous fitting of experimental data. According to Dixon's model [12], the grating decays because some modifiers are back diffusing from shallow sites and those modifiers can be caught again by the deep traps making it difficult for them to hop out. $\gamma_T \phi_0 S_T$ determines how fast the decay of the grating is. Table 2 shows that $\gamma_T \phi_0 S_T$ increases when the temperature decreases. As discussed earlier, when the temperature decreases, the densities of hot phonons and deep traps all increase. This leads to a faster decay of the grating. And at the same time, fewer thermal phonons will be generated at the lower temperature. Since these thermal phonons make it more difficult for the small mobile modifiers to move back and there are fewer thermal phonons at the low temperature, it will cause the grating to decay faster as the temperature decreases.

4.5 Temperature dependence of grating after the write beams are blocked at the maximum:

Fig. 11 shows how the grating changes with respect to time at different temperatures for the Eu8.1 sample after both write beams are blocked. Every curve is normalized by making the signal maximum 1000 arbitrary units. As soon as the diffracted signal reached the maximum, both write beams were blocked for five minutes. Then one write beam was turned on to erase the grating for two minutes. After that, the second write beam was also turned also to rewrite the grating. From Fig. 11, we know that a less persistent grating is left at higher temperature. The measurements for the samples Eu2.6, Eu3.9 and Eu5.3 show the similar trends. As discussed earlier, the density of deep trapping sites will decrease when the temperature increases. So more modifiers can hop out of the trapping potential wells and redistribute in the glass network after stopping the source of hot phonons by blocking both write beams. In this way, the weaker persistent grating was obtained at the higher temperature. However, we must keep in mind that those redistributed modifiers are still available to move and can form the grating again when both write beams are turned on.

4.6. Temperature dependence of the erasure rate:

Fig. 12 shows how the erasure rate changes as a function of time at different temperatures for the Eu5.3 sample. As stated before, the grating can be erased by a single write beam. Every curve is normalized by making the diffracted signal at the beginning of the erasure procedure one arbitrary unit. Fig. 12 shows that the decay rate increases as the temperature decreases. The measurements for the Eu2.6, Eu3.9 and Eu8.1 samples show the similar trend. To explain this, we need to note that the erasure comes from the hot phonons produced by the single write beam. The single write beam has only a

Gaussian profile that is different from the interference pattern. Thus, there is no dark region. All regions inside the beam are bright although their intensity follows a Gaussian profile. As happens during the procedure of the grating formation, the modifiers trapped in the potential wells can absorb the energy from those hot phonons and hop out of those trapping sites, and migrate in the glass network. Since there is no dark region inside the write beam volume, the modifiers redistribute again in the glass. After equilibrium is reached, the resulting change in the index of refraction does not show a periodic structure, and the grating disappears.

To consider the influence of temperature on the erasure rate, the following facts must be considered. First is that the density of hot phonons will increase as the temperature decreases. Second is the ability that the modifiers have to redistribute among the glass network. During the redistribution of the modifiers, thermal phonons will hinder their movements. Again, the density of these thermal phonons plays an important role in the erasure procedure. As presented before, their density decreases as the temperature decreases. So these two factors lead to the higher decay rate of the grating at lower temperature. But there is another factor that competes with these. That is the density of the deep trapping sites. As stated before, its density increases as the temperature decreases. Because it can make the grating more difficult to be erased, the final erasure rate will be determined by the competition of the previous two factors with it. From Fig. 12, we know the first two factors prevail.

4.7 Temperature dependence of the rewrite procedure of the grating:

Fig. 13 presents the rewrite procedure of the grating for the Eu8.1 sample at different temperatures. As presented before, the rewrite procedure occurs by turning on the second write beam after the grating was erased for two minutes by one write beam. Fig. 13 shows that a stronger rewrite grating is obtained at the higher temperatures. Similar figures are found for the Eu2.6, Eu3.9 and Eu5.3 samples. From sections 3.5 and 4.5, we know that the less persistent grating was obtained for the higher temperatures and some of the modifiers are able to move again under the illumination of both write beams. As in the previous section, to consider the influence of temperature on the rewrite procedure, we still need to consider the following facts. First is that the density of hot phonons will decrease as the temperature increases. Second is the ability that the modifiers redistribute among the glass network. During the redistribution of the modifiers, the thermal phonons will hinder their movements. As the temperature increases, higher density of thermal phonons will make the movement of modifiers more difficult. Both factors make it possible that less grating is obtained as the temperature increases. But the densities of the mobile modifiers and trapping sites compete with those two factors. Because there are more mobile modifiers and fewer deep traps at the high temperature, they can lead to a higher grating intensity as the temperature increases. From Fig. 13, we know the densities of the mobile modifiers and trapping sites prevail. So when both write beams are turned on again, a larger grating is obtained at the higher temperature.

4.8 Temperature dependence of the maximum change in index of refraction Δn_{max}:

As Figs. 14 ,15 and 16 show, the initial maximum of the change in the index of refraction varied as the temperature for the samples with different Eu concentrations and at different crossing angles. There are two trends for the different samples. For the Eu8.1 sample, the initial maximum increases as the temperature decreases. For the other Eu2.6, Eu3.9 and Eu5.3 samples, the initial maximum decreases at the lower temperature. As we know, the grating consists of two parts--persistent and transient gratings. Figs. 17 and 18 present these two parts, respectively. From Fig. 18, we know that a higher transient grating is obtained at the lower temperature. This can be understood due to the following facts. The transient component has been proven to be a population grating of the excited Eu^{3+} rare-earth modifiers [8]. According to the absorption experimental results presented by Houck [18], the density of electrons at the ground state $^7F_0$ of the Eu ions increases as the temperature decreases. So there is more absorption to the excited state $^5D_2$ for Eu ions. So the population of the excited Eu^{3+} ions in the $^5D_0$ level increases as the temperature decreases. Therefore, there is more transient grating as the temperature decreases. The same phenomenon is found for the Eu8.1 sample for the temperature range between-- $196°C$ to $27°C$.

Fig. 17 shows two opposite trends for the persistent grating. For the Eu8.1 sample, the persistent change in the index of refraction increases as the temperature decreases. For the other samples--Eu2.6, Eu3.9 and Eu5.3, it decreases at the lower temperature. Behrens *et al.* [13] reported the experiments results for their LS5 and NS5 samples. The composition of LS5 is 70.0% SiO_2, 15.0 % Li_2O, 5.0% Ba, 5.0% ZnO and 5.0 % Eu_2O_3 and NS5 consists of 70.0% SiO_2, 15.0 % Na_2O, 5.0% Ba, 5.0% ZnO and 5.0 % Eu_2O_3. As their figures show, the signal intensity increases as the temperature

decreases. That is consistent with the measurement for the Eu8.1 sample but not consistent with the other samples. The compositions of their samples are different from ours, and it is not known when they measured the signal, which is important since Fig. 2 shows the grating evolves as a function of time.

To explain these two trends, the following factors must be considered. First is that the density of hot phonons will increase as the temperature decreases. So more energy can drive more mobile modifiers to migrate as the temperature decreases. Second is the ability of the modifiers to migrate through the glass network. During the migration of mobile modifiers, the thermal phonons will hinder their movements. Again, as stated earlier, their density decreases as the temperature decreases. So those two factors can increase the persistent grating intensity as the temperature decreases. But we need to consider another factor--trapping. As we know, the density of the deep trapping sites increases as the temperature decreases. That factor can decrease the persistent grating intensity. The final result will be determined by the total influence of those three factors. It can be expected that the density of hot phonons is more important for the sample with a high Eu concentration and the density of the deep trapping sites is more important for the sample with a low Eu concentration. The two trends that Fig. 17 presents confirm these expectations.

4.9 Liquid nitrogen measurements:

According to the curves shown in Figs. 19 and 20, the signal decays very fast as soon as it reaches the initial maximum, and there is a kind of relative oscillation of the signal that is not found at the other temperatures. It seems that the signal intensity decays

to a point and then moves around it. This characteristic phenomenon is not presented in the measurement at room and above room temperature. From the curves at room temperature and above, it can be seen that the grating intensity reaches the initial maximum and decays to a constant slowly if both write beams are kept on. For the measurement at liquid nitrogen temperature, the same procedure happens, but the decay rate is much faster. This means that the grating intensity decreases to the equilibrium constant in a very short time after its maximum and then moves around this equilibrium constant. The mechanism of oscillation can be explained as follows. According to Dixon *et al.* [12], the decay of the grating intensity is attributed to the back diffusion of the mobile modifiers. At liquid nitrogen temperature, because the density of thermal phonons is much lower than that at room temperature, it can be expected that these diffused mobile modifiers can move forward again after they move back and this process can be repeated under the driving of hot phonons. And as time passes, because it is closer to equilibrium, the amplitude of the vibration decreases. Figs. 19 and 20 confirm these expectations.

CHAPTER 5

CONCLUSIONS

The results presented in Chapter 3 provide a characterization of the laser-induced grating in the Eu doped glass samples at different temperatures and at different crossing angles with different concentrations of Eu ions. The temperature varied from -196°C to 93°C. The crossing angles $2\theta_w$ are 3.87°, 5.145° and 8.75°, and the concentrations of Eu_2O_3 in the samples are 2.6, 3.9, 5.3 and 8.1 mol%. As stated earlier, the entire procedure of a typical experimental curve can be divided into writing, blocking, erasing and rewriting processes. Experiments have been performed to see how the change of temperature influences the grating for each process. The experimental data presents the following conclusions. As the temperature decreases, the build-up rate, decay rate, erasure rate and transient grating intensity increase. For the Eu8.1 sample, the persistent change in the index of refraction increases as the temperature decreases. For the other samples--Eu2.6, Eu3.9 and Eu5.3, it decreases at the lower temperature.

Dixon *et al*. [12] successfully applied the small modifier diffusion model to study the evolution of the grating at room temperature. To see the possibility that it can be applied to other temperatures during grating formation, the basic assumption needs to be examined. That is the rate of mobile ions hopping between adjacent sites is proportional to the density of the local hot phonons. As the experimental data shows, linear relations between the power of the write beam and grating growth rate at the different temperatures and different crossing angles make it possible to apply the small modifier model to other temperatures besides room temperature.

Based on the model presented by Dixon *et al.* [12], the fitting of the theoretical curves to the experimental data were done at three temperatures: $-33\,^{\circ}C$, $27\,^{\circ}C$ and $92\,^{\circ}C$. The fitting parameters are shown in Table 2. As Table 2 shows, as the temperature decreases, the density of mobile modifiers M_0 decreases. In contrast, the other three parameters--β_1, $\gamma_T\phi_0 S_T$ and $\Delta n_{transient}$ all increase as the temperature decreases. From the absorption data from Houck [18] and fluorescence data presented by Rahman [19], it can be concluded that the density of hot phonons in the sample can be expected to increase as the temperature decreases. From the experimental data presented in Fig. 25, it can be concluded that more shallow traps become deeper traps and there are more trapping sites as the temperature decreases. At the same time, another factor needs to be considered. That is the density of thermal phonons. As stated earlier, it will decrease as the temperature decreases. Based on all these factors, there is a competition among these for the formation of the laser induced grating at different temperatures. For different samples with different concentrations of Eu ions, their relative effect can be expected to be different. As the experimental data show, the increase of the density of hot phonons is more important for the sample with more Eu ions. Therefore, we are not surprised that there are two different trends exhibited by the persistent gratings for the different samples. One is that the persistent change in the index of refraction increases for the Eu8.1 sample at low temperature. Another is that the persistent change in the index of refraction decreases for the Eu2.6, Eu3.9 and Eu5.3 when the temperature decreases. It is also found that the transient change in the index of refraction increases when the temperature decreases. This can be explained by the fact that the transient grating has

been shown to be a population grating of excited Eu^{3+} rare-earth modifiers [8] and there is more absorption to the $^5D_2$ level of Eu^{3+} at lower temperatures.

Although the results described here extend the understanding of the formation of laser induced grating in Eu doped glasses, several aspects still need to be further investigated. How far the mobile modifiers can migrate still remains unknown. An additional study needs to be performed on the strange behavior of the grating evolution at the liquid nitrogen temperature. During the fitting procedure of the experimental data, it was found that the charge of the mobile modifiers was zero, which leads to the disappearance of the explicit temperature dependence. These points are not well understood and require additional investigation.

BIBLIOGRAPHY

[1] E. G. Behrens, R. C. Powell, and D. H. Blackburn, "Optical applications of laser-induced gratings in Eu doped glasses", Applied Optics **29**, 1619-1624(1990)

[2] A. Y. Hamad and J. P. Wicksted, "Holographic image storage in Eu^{3+}-doped alkali aluminosilicate glasses", Applied Optics **40**, 1822-1826(2001)

[3] G. Meltz, W. W. Morey, and W. H. Glenn, "Formation of Bragg grating in optical fibers by a transverse holographic method", Opt. Lett. **14**, 823-825(1989)

[4] E. G. Behrens, F. M. Durville, and R. C. Powell, "Observation of erasable holographic gratings at room temperature in Eu^{3+}-doped glasses", Opt. Lett. **11**, 653-655(1986)

[5] F. M. Durville, E. G. Behrens, and R. C. Powell, "Relationship between laser-induced gratings and vibrational properties of Eu-doped glasses", Phys. Rev. B. **35**, 4109-4112(1987)

[6] M. M. Broer, A. J. Bruce, and W. H. Grokiewicz, "Photoinduced refractive-index changes in several Eu^{3+}-, Pr^{3+}-, and Er^{3+}-doped oxide glasses", Phys. Rev. B. **45**, 7077-7083(1992)

[7] A. Y. Hamad, J. P. Wicksted, G. S. Dixon and L. P. deRochemont, "Laser-induced transient and permanent gratings in Eu^{3+}-doped dual alkaline earth silicate glasses", J. Of Non-crystalline Solids **241**, 59-70(1998)

[8] R. C. Powell, F. M. Durville, E. G. Behrens, and G. S. Dixon, "Linenarrowing studies of Eu^{3+} ions in glasses", J. Lumin. **40&41**, 68-71(1988)

[9] E. G. Behrens, R. C. Powell, and D. H. Blackburn, "Characteristics of laser-induced

gratings in Pr^{3+}- and Eu^{3+}-doped silicate glassess", J. Opt. Soc. Am. B **7**, 1437-1444 (1990)

[10] V. A. French, R. C. Powell, D. H. Blackburn and D. C. Cranmer, "Refractive index gratings in rare-earth-doped alkaline earth glasses", J. Appl. Phys. **69**, 913-917 (1991).

[11] A. Y. Hamad, James P. Wicksted, "Volume grating produced by intersecting Gaussian beams in an absorbing medium: a Bragg diffraction model", Optics Communications **138**, 354-364(1997).

[12] G. S. Dixon, A. Y. Hamad, J. P. Wicksted, "Kinetics of holographic refractive-index gratings in rare-earth-sensitized glasses", Phys. Rev. B. **58**, 200-205(1998).

[13] E. G. Behrens, F. M. Durville, and R. C. Powell, "Properties of laser-induced gratings in Eu-doped glasses", Phys. Rev. B. **39**, 6076-6081(1989).

[14] V. A. French, R. C. Powell, D. H. Blackburn, and D. C. Crammer, "Refractive index gratings in rare-earth-doped alkaline earth glasses ", J. Appl. Physc. **69**, 913-917(1991).

[15] J. A. Paxton, "Four-wave mixing below room temperature in Eu^{3+} doped silicate glasses", Master thesis, (1999)

[16] A. Y. Hamad, private communication, (2000)

[17] C. Kittel, "Introduction to solid state physics", 7th ed., 117(1996).

[18] M. Houck, Summer REU research report, (1999)

[19] A. Rahman, "Fluorescence and absorption measurements of europium doped aluminosilicate glasses", Master thesis, (2000).

APPENDIX

CONVERSION OF DIFFRACTED POWER TO Δn

This appendix describes the conversion of the diffracted power to the change in the index of refraction Δn based on the model presented by Hamad et al. [11].

According to Hamad et al. [11]. β is defined as the following:

$$\beta = \frac{\eta}{\Delta n^2}$$

where η is the ratio of the diffracted power and the power of the read beam. Δn is the change in the index of refraction. From the experiments, the diffracted power and the power of the read beam can be measured. Therefore, η can be calculated from the experimental data.

From the theoretical model proposed by Hamad et al. [11], we can calculate β and then obtain the change in the index of refraction Δn. Fig. 26 shows two intersecting Gaussian beams creating a volume grating pattern from Hamad et al. [11].

In the model, β is expressed as the following formula.

$$\beta = \frac{(1-R)^2 \pi^3}{2} \left(\frac{e^{-\alpha L/2}}{n_r w_r \lambda_r^2} \right)^2 \int\int (E_R^2 + E_I^2) dx dy$$

where R is the reflectivity of the sample surface and can be determined using the Fresnel equations. n_r and n_w are the refractive indexes of the sample at the wavelengths of the read beam and write beam, which are measured by using a CCD camera with a laser beam profiler in the Brewster's angle experiment. w_r is the radius of the read beam. λ_r is the wavelength of the read beam. L is the thickness of the sample. α is the absorption coefficient at the wavelength of the
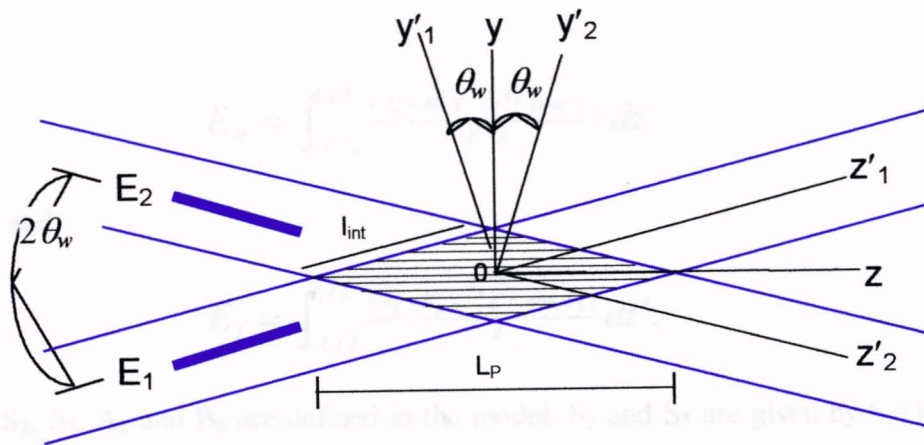
Figure 26 Two intersecting Gaussian beams creating a volume grating pattern from Hamad *et al.* [11]. The x-direction is pointing into the page.

read beam. E_R and E_I are the real and the imaginary parts of the integration over z' given by

$$E_R = \int_{-L/2}^{L/2} \frac{(A_5^2 + B_5^2)^{1/4} e^{S_2} \cos(S_3)}{z' - z} dz'$$

and

$$E_I = \int_{-L/2}^{L/2} \frac{(A_5^2 + B_5^2)^{1/4} e^{S_2} \sin(S_3)}{z' - z} dz',$$

where S_2, S_3, A_5 and B_5 are defined in the model. S_2 and S_3 are given by $S_2 = B_2 - A_2 - Sz'^2 - \alpha z'$ and $S_3 = B_1 + A_3 + S_1 z' + [\arctan(B_5/A_5)]/2$, where $S = [2(\sin\theta_w/w_w)^2 + (\sin\theta_r/w_r)^2]$, $S_1 = k_r(1 - \cos\theta_r)$. B_1 and B_2 are given by $B_1 = by^2 + \{2acd + [b(d^2 - c^2)/4A_1]\}$ and $B_2 = \{[a(d^2 - c^2) - 2bcd]/4A_1\}$, where $a = (2/w_w^2) + (1/w_r^2)$, $b = [\pi/\lambda_r(z' - z)]$, $c = (k_r\theta_r - 2k_w\theta_w - 2by)$, $d = [(\alpha_r\theta_r/2) - (2\theta_r z'/w_r^2)]$. A_5 and B_5 are given by $A_5 = (ag - b^2)/A_1(g^2 + b^2)$ and $B_5 = b(g + a)/A_1(g^2 + b^2)$. Here $A_1 = a^2 + b^2$, $A_2 = (ab^2 x^2/A_1)$, and $A_3 = (ba^2 x^2/A_1)$.

From the model, β can be evaluated numerically. After β is calculated for each sample by using a Pascal program made by Hamad et al. [11], the change in the index of refraction Δn can be deduced by using the experimental result of η.

VITA

Xiwang Zhang

Candidate for the Degree of

Master of Science

Thesis: TEMPERATURE DEPENDENCE OF LASER INDUCED GRATINGS
IN EU-DOPED GLASSES

Major Field: Physics

Biographical:

Personal Data: Born in Jingyang, Shanxi, P. R. China, On November 4, 1973, the
son of Genxu Zhang and Chunfang Dang.

Education: Received Bachelor of Science degree in optoelectronics from
University of Science and Technology of China, Hefei, Anhui. Completed
the requirements for the Master of Science degree with a major in Physics at
Oklahoma State University in August, 2001.